HHS Public Access

Author manuscript

Cell Rep. Author manuscript; available in PMC 2020 November 28.

Published in final edited form as:

Cell Rep. 2020 November 10; 33(6): 108358. doi:10.1016/j.celrep.2020.108358.

A Leptin-Mediated Neural Mechanism Linking Breathing to Metabolism

Jeehaeh Do[1], **Zheng Chang**[1,2], **Gabriella Sekerková**[1], **Donald R. McCrimmon**[1,*], **Marco Martina**[1,3,*]

[1]Department of Physiology, Northwestern University Feinberg School of Medicine, Chicago, IL 60611, USA

[2]Present address: Rosalind Franklin University of Medicine and Science, North Chicago, IL 60064, USA

[3]Lead Contact

SUMMARY

Breathing is coupled to metabolism. Leptin, a peptide mainly secreted in proportion to adipose tissue mass, increases energy expenditure with a parallel increase in breathing. We demonstrate that optogenetic activation of LepRb neurons in the nucleus of the solitary tract (NTS) mimics the respiratory stimulation after systemic leptin administration. We show that leptin activates the sodium leak channel (NALCN), thereby depolarizing a subset of glutamatergic (VGluT2) LepRb NTS neurons expressing galanin. Mice with selective deletion of NALCN in LepRb neurons have increased breathing irregularity and central apneas. On a high-fat diet, these mice gain weight with an associated depression of minute ventilation and tidal volume, which are not detected in control littermates. Anatomical mapping reveals LepRb NTS-originating glutamatergic axon terminals in a brainstem inspiratory premotor region (rVRG) and dorsomedial hypothalamus. These findings directly link a defined subset of NTS LepRb cells to the matching of ventilation to energy balance.

Graphical Abstract

*Correspondence: dm@northwestern.edu (D.R.M.), m-martina@northestwern.edu (M.M.).

AUTHOR CONTRIBUTIONS

J.D. designed and performed experiments for *ex vivo* electrophysiological recordings and cell harvesting, data analysis, viral tracing, ISH and immunohistochemical analysis, and plethysmographic analysis; developed new transgenic lines; and drafted the manuscript. Z.C. performed the *in vivo* recordings and data analysis. G.S. optimized the ISH and histochemical protocols and helped with the design of the transgenic mouse lines. D.R.M. and M.M. envisaged and directed the overall research, designed the experiments, and drafted the manuscript.

SUPPLEMENTAL INFORMATION

Supplemental Information can be found online at https://doi.org/10.1016/j.celrep.2020.108358.

DECLARATION OF INTERESTS

The authors declare no competing interests.

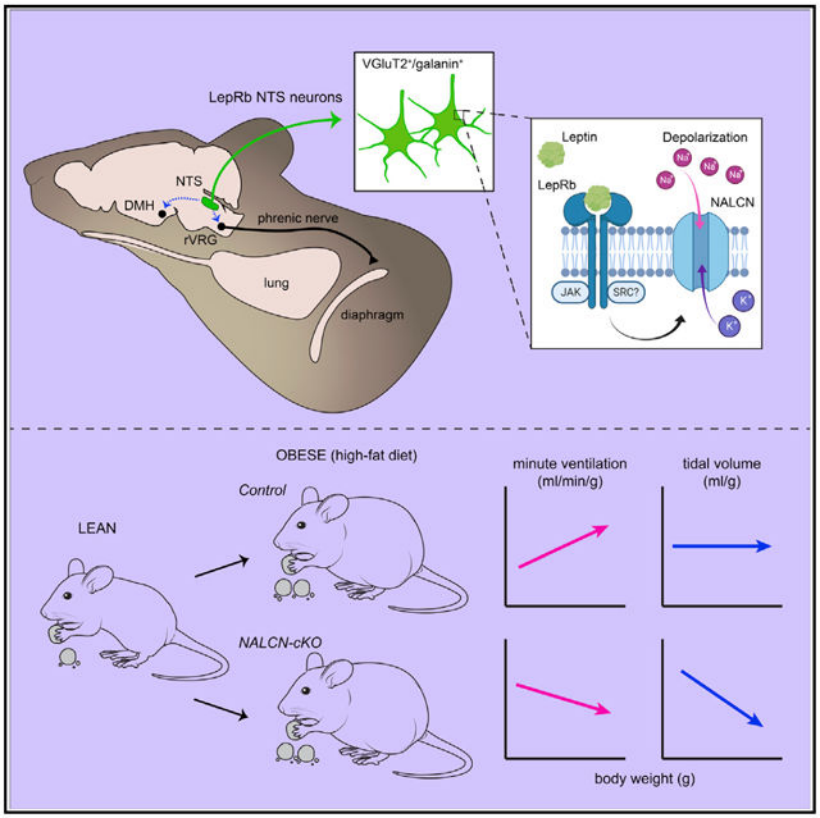

In Brief

Do et al. identify an NTS-based, leptin-dependent neural circuit that stimulates breathing, matching ventilation to energy consumption. Leptin selectively depolarizes galanin-expressing LepRb NTS neurons through activation of NALCN. Activation of this pathway is required to increase tidal volume in overweight conditions.

INTRODUCTION

The primary function of pulmonary ventilation is the regulation of arterial blood gases and acid-base status. Normal homeostasis requires that arterial CO_2 tension and pH be precisely regulated even as metabolism-driven CO_2 production changes in response to a variety of challenges (Dempsey et al., 1984) However, with the possible exception of physical exercise, in which input from type III-IV muscle afferents is important (Dempsey et al., 2014), the metabolic signals underlying this regulation and the CNS circuitry linking ventilation to metabolism have remained elusive.

In this context, one neuromodulator that has received increasing attention is leptin. Leptin is a pleiotropic hormone principally derived from adipocytes, and recent findings suggest that it may be an important signaling molecule linking ventilation to metabolism. An increase in white adipose tissue increases circulating leptin, which, in turn, induces an increase in energy expenditure (Friedman, 2019) and a parallel increase in breathing (O'Donnell et al., 2000; Bassi et al., 2016; Chang et al., 2013). Leptin-deficient *ob/ob* mice are obese,

hypoventilate with an accompanying increase in arterial PCO_2 (O'Donnell et al., 1999), and have diminished neuromuscular control of the upper airway (Polotsky et al., 2012). Leptin replacement normalizes breathing in these mice (Tankersley et al., 1996; Bassi et al., 2012, 2014; O'Donnell et al., 1999), restores neuromuscular tone in the upper airway (Polotsky et al., 2012), and relieves sleep-disordered breathing (Pho et al., 2016; Yao et al., 2016). Similarly, in humans, leptin resistance in obesity can have a role in the pathogenesis of respiratory disorders, such as obesity hypoventilation syndrome (OHS) and central sleep apnea (Donovan and Kapur, 2016; Eckert et al., 2007; Mokhlesi, 2010; Framnes and Arble, 2018).

Despite the potent effect of leptin on breathing, the cellular mechanisms of this regulation are less clear. In the periphery, there is conflicting evidence as to the potential role of carotid bodies as a site of leptin-dependent respiratory stimulation (Messenger and Ciriello, 2013; Caballero-Eraso et al., 2019; Rakoczy et al., 2018). Nevertheless, a CNS site of leptin action in the control of breathing is strongly supported because leptin administration directly into the brain augments respiratory motor output in rodents (Inyushkin et al., 2009; Bassi et al., 2015; Yao et al., 2016). In addition, the long form of the leptin receptor (LepRb), which activates intracellular signaling pathways, is localized on neurons in several discrete brain regions known to be involved in respiratory control. These include neurons in the nucleus of the solitary tract (NTS) and the hypothalamus, especially the dorsomedial hypothalamic nucleus (DMH; Fukushi et al., 2019). Of these, the most strongly linked to the control of breathing is the NTS. Injection of leptin into the NTS of rats stimulates respiratory motor output (Inyushkin et al., 2009; Inyushkina et al., 2010). Additionally, Yao et al. (2016) compared the effect on breathing of leptin administration into the fourth, versus a lateral, ventricle of *ob/ob* mice and found that the fourth ventricle, but not lateral ventricle, administration stimulated respiratory drive, presumably by activating medullary, probably NTS, leptin receptors.

The cellular mechanisms by which leptin alters neuronal excitability have been examined in several cell types. For example, leptin reportedly hyperpolarizes neuropeptide Y-expressing hypothalamic neurons and pancreatic β-cells through activation of ATP-sensitive K channels (K_{ATP}; Spanswick et al., 1997; van den Top et al., 2004) and hippocampal neurons by activation of calcium-activated potassium (BK) channels (Shanley et al., 2002). However, the opposite effects were also described, even in the same brain areas, because leptin was also found to depolarize hippocampal neurons, as well as pro-opiomelanocortin (POMC)-expressing hypothalamic neurons, by activating transient receptor potential-canonical (TRPC) channels (Qiu et al., 2010; Dhar et al., 2014). Further, in hippocampal neurons, leptin alters neuronal excitability by enhancing synaptic plasticity through modulation of NMDA receptor (NMDAR) function (Shanley et al., 2001; Moult and Harvey, 2011). Both the excitatory and inhibitory actions are dependent on the intracellular JAK/STAT, PI3K, and MAPK signaling pathways (Gavello et al., 2016). Even within the NTS, both excitatory (Hisadome et al., 2010) and inhibitory (Williams and Smith, 2006) effects have been reported, and the inhibitory effect was suggested to depend on K_{ATP} channels (Williams and Smith, 2006). The possible mechanisms of the excitatory responses remain unexplored. Thus, although NTS neurons expressing LepRb (LepRb NTS neurons) are good candidates for stimulating breathing, whether that occurs via excitatory or inhibitory mechanisms is

unknown as are the identities of ion channels mediating the change in NTS neuron excitability and the neuronal network involved.

Here, we exploit the complementary strengths of *ex vivo* and *in vivo* approaches to identify the cellular and network mechanisms mediating respiratory stimulation by leptin. We find that leptin depolarizes a subgroup of LepRb NTS neurons containing both the glutamate transporter (VGluT2) and galanin via activation the sodium leak channel (NALCN). We further show that these neurons directly project to the region containing bulbospinal inspiratory premotor neurons, the rostral ventral respiratory group (rVRG), the ventrolateral medulla, and the DMH. Selective deletion of NALCN in LepRb neurons results in an increase in spontaneous apneas and breathing irregularity as well as a decrease in CO_2 chemosensitivity. Furthermore, although control mice fed a high-fat diet (HFD) for 3 weeks maintain constant minute ventilation relative to body weight, LepRb-selective NALCN-knockout (KO) mice show a marked depression in ventilation compared with their lean state. Thus, our data identify a population of glutamatergic, galanin-expressing LepRb NTS neurons as a key component of a leptin-dependent circuit that links metabolism to breathing.

RESULTS

Optogenetic Activation of LepRb NTS Neurons Stimulates Respiratory Motor Output

We first asked whether LepRb NTS neurons could stimulate breathing. To test that, we developed a mouse line in which ChR2 (channelrhodopsin-2) fused to EYFP (enhanced yellow fluorescent protein; ChR2/EYFP) was selectively expressed in LepRb neurons (LepRb-Cre::loxP-ChR2/EYFP, i.e., $ChR2^+$; Figures 1A and S1). Immunostaining confirmed the expression of membrane bound ChR2/EYFP (Figure 1B). Further, double labeling of LepRb mRNA (in situ hybridization histochemistry [ISHH]) and EYFP immunostaining (see representative image in Figure 1C) showed that, in the NTS, all $EYFP^+$ cells expressed LepRb mRNA, whereas $EYFP^+$ cells represented 42% ± 4.4% of LepRb NTS neurons. These results demonstrate that ChR2 expression in the NTS of our mouse line is completely selective, although with incomplete penetrance and, thus, can be used for selective optogenetic activation.

Recordings in acute brainstem slices confirmed that light (488 nm) stimulation excited LepRb NTS neurons (Figures S1E and S1F) and that 20-Hz trains of optical stimuli elicited repetitive firing throughout a 1-min stimulation period (Figure S1G). To test the effect of activating NTS LepRb neurons on respiratory motor output (i.e., phrenic nerve discharge) in anesthetized mice, an optical fiber was placed on the dorsal surface of the brainstem directly above the medial NTS at the level of calamus scriptorius ± 600 μm (Figures 1D and S1B). In anesthetized $ChR2^+$ mice, five or six trains of light stimuli (each train consisted of 1 min of 10 ms duration, 20 Hz, 4 mW/mm^2 light pulses) produced a transient reduction in phrenic burst rate (*f*, fictive breathing frequency) during the period of stimulation, with no effect on the peak amplitude of the integrated phrenic activity (fictive tidal volume [V_T]; Figures 1E, 1I, and 1J). After the end of each stimulation period, the phrenic-burst frequency rapidly returned to baseline. Then, beginning 11 ± 3.5 min after the onset of the first stimulus train, there was a slow, progressive increase in the peak amplitude of ∫Phr, reaching an ~150% increase at 35 ± 6.7 min after the onset of the first stimulus train (Figures 1E, 1H, and 1K).

This average increase was maintained during the 60-min recording period in the nine mice tested (Figure 1H), although, in three mice, the increase was maintained for less than 60 min (e.g., Figure 1E). $ChR2^{-}$ control littermates did not exhibit either the acute inhibition of the burst frequency (Figure 1I) or the longer-term increase in the burst amplitude (Figure 1L). There was no sustained change in burst frequency in either control or $ChR2^{+}$ mice (Figure 1G). These results show that selective, unilateral activation of a subset (~42%) of LepRb NTS neurons expressing ChR2 is sufficient to increase tidal volume robustly after transient inhibition of breathing frequency.

Intrinsic Electrophysiological Properties Identify Two Types of LepRb NTS Neurons

The intrinsic properties of LepRb NTS neurons were examined with patch clamp recordings in acute brain slices (Figure 2A). We soon found that these neurons could be classified into two electrophysiologically distinct populations that could be selected according to somatic size. Smaller cells (defined as type 1) showed spike-frequency adaptation, rebound firing, and their action potentials were followed by small afterdepolarizations; larger (type 2) cells, in contrast, had a delayed onset of firing, fired regularly with no rebound firing, and their action potentials featured prominent afterhyperpolarizations (Figures 2B, 2C, and 2E). Other differences between the two cell types included action potential threshold, membrane resistance and capacitance (Figures 2F to 2I), and the input and output curve (Figure 2J). Type-1 and type-2 cells were intermixed within the medial region of the NTS at the rostrocaudal level of the area postrema and commissural NTS (Figure 2D).

We hypothesized that specific molecular markers distinguish type-1 from type-2 LepRb NTS neurons. To test this hypothesis, type-1 and type-2 cells, visually selected based on apparent somatic size, were patched, their identity was confirmed by their electrophysiological properties, and their cytoplasm was harvested for single-cell RNA sequencing (GEO: GSE158582). Unsupervised cluster analysis of the transcripts revealed that type-1 and type-2 cells had distinct molecular profiles (Figure 2K). Type-1 cells contained the VGluT2 and expressed the neuropeptide galanin, which is abundantly expressed in the dorsal-vagal complex (Pérez et al., 2001). Most type-2 cells also contained VGluT2, but they selectively expressed the prolactin receptor (*prlr*) and displayed a greater transcription level of the glucagon gene (*gcg*), which encodes the precursor mRNA for glucagon-like peptide 1 (GLP-1) (Figures 2L and S2A). Type-2 cells that did not contain VGluT2-mRNA-expressed choline acetyltransferase mRNA (*chat*), a marker for cholinergic neurons (Figures 2K and S2). These cholinergic cells (n = 2) were collected near the border of the dorsal motor nucleus of the vagus (DMV) and presumably represented vagal motoneurons.

LepRb NTS neurons were distributed along the rostrocaudal axis of the caudal NTS (Figure S3A). To further investigate the peptide expression profile of LepRb NTS neurons, we performed double in situ hybridization histochemistry (ISHH) for LepRb and selected peptide transcripts on serial brain sections. In these experiments, galanin was expressed in 61.1% ± 2.6% (n = 3 mice) and GLP-1 in 18% ± 1.5% (n = 3 mice) of the whole LepRb NTS population (Figures S3B and S3C). Importantly, there were no overlapping expressions of galanin and GLP-1 in the NTS (Figure S3E), which further supports the complete segregation of type-1 and type-2 cells. Cholecystokinin (CCK), which is also known to be

prominently expressed in NTS neurons (Garfield et al., 2012), was only present in 4.7%± 1.0% (n = 3 mice) of LepRb NTS cells (Figure S3D). However, because the population of LepRb NTS neurons expressing either galanin or GLP-1 was <100% of the total LepRb neurons, we cannot exclude the presence of, at least, a third population of LepRb NTS neurons. In addition, some neurons near the border of the DMV might represent vagal motoneurons intermingled with NTS neurons (see above) and, thus, might account for a portion of the LepRb-labeled cells. Lastly, in keeping with a previous report (Huo et al., 2006), we did not detect any co-expression of POMC in LepRb NTS neurons.

What Is the Electrophysiological Effect of Leptin on NTS Neurons?

So far, we have identified two populations of LepRb NTS neurons (excluding the presumed vagal motoneurons) that are glutamatergic but are distinguished by expression of different neuropeptides and have demonstrated that selective optogenetic stimulation of LepRb NTS neurons potentiates the amplitude of the phrenic nerve output. However, the effect of leptin on the excitability of LepRb NTS neurons is controversial. Several authors have documented leptin-mediated activation of NTS neurons (Elias et al., 2000; Huo et al., 2007; Hisadome et al., 2010). In contrast, Williams and Smith (2006) reported that leptin hyperpolarizes a fraction of NTS neurons through activation of potassium conductance, although those findings are not mutually exclusive. Because we identified two populations of LepRb NTS neurons with different electrophysiological properties, we sought to determine whether the effect of leptin differed in those two cell types by recordings in acute slices. We found that leptin depolarized 16 of 19 type-1 cells (**$p < 0.01$; 4.07 ± 0.86 mV; Figures 3A and 3B). In the remaining three type-1 cells, leptin had no measurable effect. Type-2 cells did not show any detectable response to leptin application, at least within the time course examined with our slice recordings (Figures 3C and 3D).

Although our data, which show either depolarization (type-1 cells) or no effect (type-2 cells) in response to leptin, are consistent with much of the literature, we never observed hyperpolarization. The reason why we never observed K_{ATP}-channel-dependent hyperpolarizing responses (Williams and Smith, 2006) is not clear. Similar inconsistencies, particularly in current clamp recordings, often depend on small differences in intracellular solutions; thus, this observation raised another critical question: what is the leptin effect on intact neurons? To answer that, we performed gramicidin perforated-patch recordings, which allowed recording without disrupting the endogenous ATP concentration. Similar to our whole-cell data, leptin induced a depolarization in type-1 cells and increased their spontaneous firing rate (*$p < 0.05$; Figure S4). Thus, in agreement with the excitatory effects observed *in vivo*, leptin depolarizes type-1 LepRb NTS neurons in the presence of physiological intracellular ATP.

Activation of the NALCN Is Required for Leptin Stimulation of Respiratory Motor Output

Next, we sought to identify the conductance mediating the leptin-induced depolarization in type-1 cells. Initial experiments demonstrated that the response to leptin was similar using either whole-cell or perforated-patch recordings. Thus, for experiments to characterize the underlying conductance, we used the whole-cell configuration, which allows precise control of the intracellular ionic concentrations. Leptin activated a cationic conductance (reversal

potential −7.7 ± 2.8 mV; Figures 3E–3G), which was blocked by gadolinium (Figure 3H) as well as by substituting *N*-methyl-D-glucamine (NMDG) for extracellular sodium (Figure 3I). These properties resemble those of NALCN channels, which have previously been shown to mediate NK1-receptor-dependent current in the retrotrapezoid nucleus, a region contributing to respiratory-related chemoreception (Shi et al., 2016). Because no selective pharmacological tools are available to assess NALCN-mediated currents, we created a mouse line that lacked NALCN expression in LepRb neurons (NALCN conditional KO [NALCN-cKO] mice). ISHH confirmed that no NALCN expression was detectable in the LepRb NTS neurons of these mice (Figure 4A). Patch clamp recordings revealed that type-1 cells lacking NALCN showed no detectable differences in resting membrane potential or membrane resistance compared with their control counterparts (Figure 4B). Importantly, type-1 cells in NALCN-cKO mice completely lacked any depolarizing response to leptin (Figures 4C and 4D), supporting the hypothesis that, in near-physiological conditions, the depolarizing effect of leptin in type1 cells is mediated by activation of NALCN. In contrast, type-2 cells of NALCN-cKO mice were hyperpolarized and had increased membrane resistance compared with control counterparts (Figure 4B). Additionally, in control mice, extracellular gadolinium slowed the spontaneous firing frequency of type-2 cells (Figure S4). Taken together, these observations suggest that, in type-2 cells, NALCN provides a background current that facilitates spontaneous firing but does not mediate a leptin response under our experimental conditions.

Because the leptin-mediated depolarization of type-1 LepRb NTS neurons requires NALCN, we hypothesized that leptin-mediated stimulation of tidal volume also requires NALCN. To test that hypothesis, we compared the effect, on phrenic motor output, of leptin injections into the NTS of anesthetized control and NALCN-cKO mice. In both groups, post hoc immunostaining of brain sections confirmed leptin-induced phosphorylation of STAT3 (pSTAT3; Figure S5). Hence, successful injections were confirmed by histological analysis of pSTAT3 and cFos expression (Figure S5). In control animals, leptin caused a slow, long-lasting increase in integrated phrenic amplitude and a transient increase in phrenic burst frequency (Figure 4E), confirming the previously reported respiratory response to leptin injections in the NTS (Inyushkin et al., 2009). In NALCN-cKO mice, however, the effect of leptin was completely abolished (Figure 4F) supporting our hypothesis that NALCN expression in type-1 LepRb NTS neurons is necessary for NTS leptin-mediated stimulation of breathing.

Selective NALCN KO in LepRb Neurons Alters Breathing Patterns

Unlike global NALCN deletion (Lu et al., 2007) or selective deletion in excitatory pre-Bötzinger complex neurons (Yeh et al., 2017), no neonatal lethality was observed in NALCN-cKO mice. Additionally, there were no differences in body weight (control versus KO, 28.8 ± 1.1 versus 30.2 ± 2.0 g) or body temperature (control versus KO, 35.5 ± 0.9 versus 35.7 ± 0.9°C) compared with age-matched control littermates. In addition, during quiet, wakeful, unrestrained breathing, we found no difference in tidal volume (V_T), breathing frequency (f), or minute ventilation (V_E; Figures 5A, 5B, 5J, and 5K). However, NALCN-cKO mice exhibited significant increases in several measures of breath-to-breath variability in breathing patterns. There was an increase in spontaneous central apneas

(Figure 5D), and Poincaré analysis (Figure 5C) revealed an increase in the breath-to-breath variability in respiratory frequency (SD1, $p = 0.034$) as well as long-term variability in respiratory frequency over the recorded interval (SD2, $p = 0.053$; Figures 5E and 5F). In addition, the coefficient of variation (CV) for all breaths (excluding apneas) was increased (Figure 5G), as was the breath-to-breath interval irregularity (Figure 5H). Thus, the main effect of NALCN deletion in LepRb neurons was an increase in irregularity with an associated increase in central apneic events in baseline eupneic breathing.

Leptin is also known to increase CO_2 chemosensitivity (Bassi et al., 2012, 2014; Tankersley et al., 1996), although its effect on peripheral chemoreception is controversial with either increases or no change in sensitivity reported (Caballero-Eraso et al., 2019; Rakoczy et al., 2018). To determine whether NALCN deletion in LepRb neurons attenuates chemosensitivity, we determined the ventilatory response to chemoreceptor stimulation (5% CO_2 or 10% O_2) in lean NALCN-cKO versus control mice (Figure 5I). In NALCN-cKO mice, the hypercapnic response was reduced (Figure 5K), but there was no detectable difference in the response to hypoxia (Figure 5J).

High-Fat Diet Stimulates Minute Ventilation via Leptin-Sensitive NALCN Channels

The above data were obtained in lean mice, a condition in which the basal level of leptin is relatively low; that may contribute to the comparatively small ventilatory effects in NALCN-cKO mice relative to the excitatory responses induced by excitation of LepRb NTS neurons (Figures 1 and 4). This suggests that the NTS LepRb-NALCN-dependent network may become more important when leptin levels are increased, such as in animals with greater adiposity. Therefore, we hypothesized that the absence of NALCN should prevent adaptive increases in minute ventilation as mice gain weight and increase leptin production in response to a HFD (Figure 6A). A HFD for 3 weeks increased circulating leptin about 10-fold in both control and NALCN-cKO mice (3.7 ± 1.2 ng/mL to 43.4 ± 7.5 ng/mL in control and 5.4 ± 2.2 ng/mL to 52 ± 9.0 ng/mL in NALCN-cKO; Figure S6I). This time frame was short enough to avoid the emergence of significant leptin resistance (as assessed by measuring pSTAT3 response to leptin injections intraperitoneally [i.p.], 3 mg/kg; not shown). In our experiments, a HFD caused no difference in either weight gain or plasma leptin concentration between control and NALCN-cKO mice (Figures 6B, S6I, and S6J).

A HFD, however, induced breathing adaptations that differed among the two genotypes (Figure 6). The findings are presented as the correlation between body weight and minute ventilation, tidal volume, and breathing frequency (Figures 6C, 6E, and 6G), irrespective of the duration of the HFD. An alternative presentation in Figures 6D, 6F, and 6H illustrates minute ventilation, tidal volume, and breathing frequency normalized to their pre-HFD values and plotted at 0, 1, and 3 weeks of a HFD. Both presentations highlight the negative effect of NALCN-cKO on minute ventilation and tidal volume with a HFD. The most striking finding was that, although control mice exhibited a mild positive correlation between body weight and minute ventilation (Figure 6C), there was an inverse correlation between body weight and minute ventilation in NALCN-cKO mice. The positive correlation in control mice was driven by a positive correlation between weight and breathing frequency (Figure 6H) with no significant effect of tidal volume (Figure 6F). In contrast, the negative

correlation between body weight and minute ventilation in NALCN-cKO mice was the result of a significant inverse relationship between tidal volume and body weight (Figure 6F). For breathing frequency, there was a similar positive correlation between body weight and breathing frequency in both control and NALCN-cKO mice (Figure 6H).

LepRb NTS Neurons Provide Excitatory Inputs to Respiratory Premotor Neurons

Our data show that leptin potentiates phrenic motor output by a NALCN-dependent depolarization of type-1 LepRb NTS neurons. We then asked how the excitation of LepRb NTS neurons is relayed to bulbospinal inspiratory premotor neurons, which are concentrated in the rVRG. To do so, an anterogradely transported Cre-dependent adeno-associated virus (AAV) was injected into the NTS of LepRb-Cre mice (Figures 7A and 7B). Anterograde labeling was identified in the ventral medulla, particularly in the region of the rVRG (Figure 7C). In additions, projections were verified in the DMH (Figure 7E). Double labeling of the AAV-reporter mCherry with VGluT2 further confirmed glutamatergic projections to both the region of the rVRG (Figure 7D) and the DMH (Figure 7F), which is also known to modulate respiratory control (McDowall et al., 2007; Yao et al., 2016). Thus, potentially, both mono- and poly-synaptic pathways convey LepRb NTS neuron excitation to respiratory premotor neurons. These data suggest that LepRb NTS neurons provide a glutamatergic pathway that relays excitation to premotor breathing control areas.

DISCUSSION

Leptin is a potent respiratory stimulant, and the NTS is a key brain region mediating that effect. Our study demonstrates that NTS activation by leptin is mediated by a subset of glutamatergic (VGluT2 containing) LepRb NTS neurons that co-express the peptide marker galanin. Further, we show that leptin stimulation of these neurons occurs by activation of NALCN. Accordingly, deletion of NALCN prevented the potentiation of respiratory motor output in anesthetized mice after injection of leptin directly into the NTS; it also disrupted body-weight-dependent homeostatic regulation of breathing. That is, lean, awake, unrestrained mice lacking NALCN in LepRb neurons exhibited an increase in breathing irregularities and spontaneous apneas and decreased hypercapnic ventilatory responses. Placing those mice on a HFD for 3 weeks reduced tidal volume and minute ventilation as a function of body weight. Finally, the neural circuit underlying these respiratory effects may involve both a direct pathway from the type-1 LepRb NTS neurons to the region of inspiratory premotor neurons in the rVRG as well as an indirect route through the DMH. Thus, type-1 LepRb NTS neurons process the leptin signal, which is intrinsically related to metabolism and energy balance, through the activation of NALCN and communicate it to respiratory neurons controlling tidal volume.

Because ventilation must parallel energy expenditure for arterial blood gas homeostasis, there must be areas of the CNS in which the circuitry controlling these two systems converge. NTS LepRb neurons and glia contribute to interactions of energy balance with gastrointestinal (GI) satiation signaling (Myers et al., 2009; Hayes et al., 2010; Stein et al., 2020). Because the NTS is also a major chemosensitive area that regulates breathing (Nattie,

2001; Huda et al., 2012), it appears ideally suited to harmonize these multiple functions with body-mass-related respiratory control and CO_2 chemosensitivity.

Optogenetic Activation of LepRb NTS Neurons

Optogenetic stimulation selectively activates LepRb NTS neurons, thereby demonstrating that activation of these neurons is sufficient to induce the sustained increase in respiratory motor output. Although this approach has the limitation of likely increasing neuronal firing more than endogenously released leptin would, the magnitude and time course of the respiratory motor response are similar to that in mice given leptin either systemically (Chang et al., 2013) or directly into the NTS (Figure 4; Inyushkin et al., 2009). The slow, progressive increase in phrenic nerve discharge after optogenetic activation of LepRb NTS neurons which, in most (6 of 9) mice, was sustained for at least 1 h is suggestive of the development of plasticity and is similar to the induction of phrenic motor facilitation after a variety of triggers, such as three, 5-min exposures to mild hypoxia (Hayashi et al., 1993; Fields and Mitchell, 2015). The cellular mechanism(s) underlying this slow, progressive increase in phrenic nerve discharge is of considerable interest but was beyond the scope of the current investigation.

The transient decrease in phrenic nerve burst frequency that occurred during optogenetic stimulation is also interesting. A possible explanation is that type-2 LepRb NTS neurons, which express GAD2 as well as VGluT2, release GABA when heavily stimulated and project to pre-Bötzinger complex neurons involved in generation of the inspiratory rhythm (Del Negro et al., 2018; Baertsch et al., 2018). Alternatively, it could also arise from the excitatory projection to the rVRG because we have previously shown that excitation of the rVRG with nanoliter injections of an excitatory amino acid produces bradypnea (Monnier et al., 2003). A third possibility that we cannot rule out is that the bradypnea and apnea could arise via projections relayed through either the parabrachial pons or the hypothalamus.

Differential Role of NALCN Channels in LepRb NTS Neurons

Our data show that the leptin-induced depolarization in type-1 cells was abolished in NALCN-cKO mice. However, NALCN channels are also expressed in type-2 cells, which did not respond to leptin application in the slice. The simplest interpretation of these data is that NALCN is coupled with LepRb in type-1 cells, whereas, in type-2 cells, it is a background conductance facilitating spontaneous firing, as reported for other neurons (Flourakis et al., 2015; Lutas et al., 2016; Yeh et al., 2017). This is supported by the observation that, in NALCN-cKO mice, type-2 cells are hyperpolarized and have greater resistance compared with cells from control mice. In type-1 cells, in contrast, NALCN did not mediate a background conductance under our experimental conditions because neither resting membrane potential nor input resistance differed between the control and the NALCN-cKO groups. Rather, the NALCN conductance was entirely leptin dependent.

NALCN is a nonselective cation channel (Ren, 2011), and thus, its opening has a net depolarizing effect. Previous studies have shown that substance P and neurotensin activate NALCN; both neuropeptides bind to G-protein-coupled receptors. However, LepRb is a cytokine receptor; thus, we can only speculate as to the coupling mechanism. NALCN has

been suggested to be activated through a G-protein-independent, Src family kinase (SKF)-dependent pathway (Lu et al., 2007; Wang and Ren, 2009; Ford et al., 2018; Swayne et al., 2009). Because leptin activates Src family kinases (Jiang et al., 2008; Baver et al., 2014; Heida et al., 2010), this may be the mechanism by which leptin modulates NALCN.

Leptin Modulation of Breathing

The endogenous effect of leptin on breathing was determined by comparing control with NALCN-cKO mice. Although the respiratory changes in NALCN-cKO mice were subtle, they supported the role of endogenous leptin in lean mice and the relatively greater effect in the respiratory pathophysiology associated with weight gain during a HFD. These *in vivo* findings in NALCN-cKO mice may underestimate the overall role of CNS leptin on the control of breathing because leptin activates NALCN in only a subset of LepRb NTS neurons. If type-2 LepRb NTS neurons contribute to the control of breathing or if LepRb neurons in other CNS sites contribute, the aggregate effect of leptin on breathing could be significantly stronger.

The increased respiratory drive observed after either leptin injection into the NTS or optogenetic activation of LepRb NTS neurons is also consistent with the previously reported leptin-dependent increase in CO_2 chemosensitivity (Bassi et al., 2012, 2014; Tankersley et al., 1996) because NALCN-cKO animals exhibited a decrease in CO_2 chemosensitivity. A contribution of LepRb NTS neurons to CO_2 chemosensitivity is also consistent with previous reports showing that ~40% of NTS neurons are intrinsically chemosensitive (Huda et al., 2012; Fu et al., 2017). Interestingly, Fu et al. (2017) reported that about 43% of NTS Phox2b-expressing (presumably glutamatergic [Kang et al., 2007]) neurons are chemosensitive and that selective ablation of a subset of NTS Phox2b neurons that express the NK1 receptor with the neurotoxin saporin attenuated the CO_2 response.

The fact that breathing is regulated by a chemosensitive feedback, however, is also relevant to the overall interpretation of the leptin effect on breathing. Leptin increases energy expenditure (Friedman, 2019) and any increase in metabolism that is not matched by a parallel increase in alveolar ventilation results in an increase in arterial PCO_2, which, in turn, will stimulate respiratory motor output independent of any direct respiratory action by leptin. In the current experiments, metabolism was not directly measured, which imposes a possible limitation. However, two complementary observations support the idea that leptin modulation of breathing is not simply the result of increased metabolism. First, in the anesthetized mice, end-tidal PCO_2 was maintained constant by adjusting the inspired fraction of CO_2 in the inspired gas to maintain a constant end-tidal PCO_2 (see STAR Methods). Second, in the plethysmography experiments, abdominal temperature provided a general indicator of metabolism, and it did not differ between lean control and NALCN-cKO mice.

To our surprise, we did not detect a change in the ventilatory response to hypoxia in awake, lean NALCN-cKO mice. Because hypoxia is largely sensed by peripheral chemoreceptors, this further supports that the observed decrease in CO_2 sensitivity occurred via a change in CNS chemosensitivity. Nevertheless, the lack of effect on hypoxia sensitivity is surprising because carotid body glomus cells express LepRb (Porzionato et al., 2011). Additionally,

exogenous leptin reportedly enhances ventilatory responses to hypoxia in mice (e.g., Caballero-Eraso et al., 2019; but see Rakoczy et al., 2018). Our lack of an effect on the hypoxic response could arise if LepRb in carotid body cells, such as in type-2 cells, are not coupled with NALCN. The lack of effect also suggests that type-1 cells are not major targets of the carotid chemoreceptor input to brainstem respiratory circuitry, and/or the baseline endogenous leptin level in lean mice is not sufficient to elicit a change in the gain of the hypoxic ventilatory response.

The Role of Leptin in Obesity-Related Breathing Disorders

NALCN-cKO mice exhibited increased breathing irregularities, with an increase in central apneas compared with control littermates. These changes may be indicators of subtle changes in respiratory control during the awake state and suggest that disruption of signaling in LepRb NTS neurons could contribute to sleep-disordered breathing in which there is increased breathing irregularity along with a reduction in upper airway tone. This interpretation extends the conclusions of Yao et al. (2016), who examined leptin effects on sleep-disordered breathing in *ob/ob* mice and found that disordered breathing was alleviated by leptin injections into the lateral, but not the fourth, ventricle and attributed the effect to the DMH, which they found projects directly to the upper airway motoneurons. However, our data demonstrate a projection from glutamatergic LepRb NTS to the DMH, thereby providing a potential pathway from the NTS that could alleviate obstructive apneas. Thus, our data suggest that NTS LepRb neurons contribute to the stability of the respiratory pattern and reduce the occurrence of both central and obstructive apneas. These considerations further suggest that leptin modulation may have a central role in obesity-related breathing disorders.

The obesity-associated increased risk of breathing disorders has typically been attributed to mechanical causes, such as fat storage in pharyngeal tissue or decreased neuromuscular tone in the upper airway; however, it has become clear that a blunted central respiratory drive is also critical (Leech et al., 1991). In line with this interpretation, common breathing disorders in individuals with obesity include OHS and sleep-disordered breathing (Bassi et al., 2016; Piper and Grunstein, 2011). The latter includes central sleep apnea, which is a failure of the CNS to generate a respiratory motor output (Eckert et al., 2007). Patients with OHS are hypoxemic and hypercapnic during the daytime (Mokhlesi, 2010); intriguingly, these patients have significantly higher circulating levels of leptin compared with lean or BMI-matched subjects without obstructive sleep apnea (Campo et al., 2007). However, not all individuals with obesity develop central leptin resistance, and many individuals with obesity do not develop OHS. In fact, individuals with obesity who are eucapnic show an increased neuronal drive for breathing (Burki and Baker, 1984; Steier et al., 2009). One can speculate that, in individuals with obesity not experiencing leptin resistance, leptin provides a mechanism to stimulate breathing and counterbalance the negative mechanical and metabolic effects caused by obesity (Chlif et al., 2009; Steier et al., 2014). In keeping with that hypothesis, we found the main respiratory effect caused by activation of LepRb NTS neurons was an increase in tidal volume or its neural equivalent, a peak amplitude of integrated phrenic nerve activity. We suggest that this effect results from the leptin-dependent, NALCN-mediated depolarization of glutamatergic neurons that project to the

rVRG. Because the rVRG is the site of premotor neurons that control phrenic motor output, the primary result of such activation is a potentiation of the peak amplitude of integrated phrenic motor activity. Accordingly, we did not find terminals of LepRb NTS neurons in respiratory rhythm-generating areas (i.e., the pre-Bötzinger complex or the parafacial and retrotrapezoid nucleus (Del Negro et al., 2018). Also consistent with this interpretation was the finding that the major influence on breathing in NALCN-cKO mice was on tidal volume.

Thus, our data identify LepRb NTS neurons as a source of the respiratory drive that helps individuals with obesity who are eucapnic maintain normal arterial blood gases. Such a mechanism was proposed 50 years ago when a clinical study found that people with obesity who were hypercapnic, compared with counterparts with normal blood gases, show “an incapacity to increase the activity in the respiratory muscles to levels necessary to overcome the load caused by obesity” (Lourenço, 1969). Although it is well known that leptin ameliorates the hypoventilation observed in obese mice lacking circulating leptin (O’Donnell et al., 1999), our findings identify type-1 LepRb NTS neurons as the first element in a network underlying that modulation and the NALCN-dependent depolarization as the critical cellular mechanism involved.

STAR★METHODS

RESOURCE AVAILABILITY

Lead Contact—Further information and requests for resources and reagents should be directed to and will be fulfilled by the Lead Contact, Marco Martina (m-martina@northwestern.edu).

Materials Availability—There are restrictions to the availability of LepRb-Cre::loxP-TdT::loxP-NALCN (NALCN KO) mice due to an MTA with Dr. Deijen Ren, University of Pennsylvania.

Data and Code Availability—The accession number for the single-cell patch RNA-sequencing data in this paper is Gene Expression Omnibus (GEO): GSE158582. The MATLAB codes supporting the current study are available from the corresponding authors on request.

EXPERIMENTAL MODEL AND SUBJECT DETAILS

Mice—LepRb-Cre mice (stock 008320), Ai32 mice (stock 021569), and Ai39 mice (stock 014539) were purchased from Jackson Laboratories. loxP-Tdt::loxP-NALCN mice were a gift from Dr. Deijen Ren (UPenn). Experiments were approved by the Northwestern University Institutional Animal Care and Use Committee (IACUC) in accordance with NIH guidelines. All mice were subject to regular veterinary inspection and only to the experimental procedures detailed here and maintained on a conventional 14hr light/10hr dark cycle with free access to food and water. Littermates of the same sex were assigned equally and randomly to treatment groups.

For *in vivo* phrenic nerve recording studies, both male and female, 3 to 8 month-old $ChR2^+$ mice were used. $ChR2^+$ mice were generated by crossing LepRb-Cre mice with Ai32 mice

This crossing resulted in 50% chance of yielding offspring expressing homozygous ChR2/EYFP fusion protein in LepRb neurons (see Figure S1). The remaining 50% of the progeny with no Cre expression were used as control animals.

For *ex vivo* patch clamp studies, male and female, 1 to 3 month-old Halo$^+$ mice were used. Halo$^+$ mice were generated by crossing LepRb-Cre mice with Ai39 mice. This crossing resulted in 50% chance of yielding offspring expressing homozygous eNpHR3.0/EYFP fusion protein in LepRb neurons (see Figure S1). The remaining 50% of the progeny with no Cre expression were used as control animals.

For *in vivo* plethysmography studies, only male mice of aged 3–5 months aged were used. Female mice were excluded from these experiments as female mice had less weight gain by HFD feeding, and rarely settled into quiet, wakefulness required for breathing measurements. Male mice were group housed (3 mice/cage) and had free access to either control diet or HFD. NALCN-cKO mice were generated by crossing LepRb-Cre mice with loxP-Tdt::loxP-NALCN mice. Breeding resulted in 37.5% chance of yielding offspring that lacked NALCN expression in LepRb cells. The expected lack of NALCN expression was confirmed by ISHH in sections encompassing multiple brain regions. 50% of the progeny that had no Cre expression were used as control animals.

The specific expression pattern of all transgenic mouse lines used in this study was confirmed by immunohistochemistry and/or *in situ* hybridization histochemistry (ISHH) in the sections encompassing multiple brain regions. Our expression data was comparable to the ISH data of the mouse Allen Brain Atlas.

METHOD DETAILS

Reagents—Unless otherwise reported, all reagents were purchased from Millipore-Sigma. Antibodies and ISHH probes used in this study are listed in the Key Resources table. Viral reagents were purchased from Addgene. The Cre-dependent viral construct, Paav-hSyn-DIO-hM4D(Gi)-mCherry, was a gift from Dr. Bryan Roth (Addgene viral prep # 44362-AAV9; http://addgene.org/44362; RRID: Addgene_44362). The DREADD construct was packaged in an AAV-serotype-9 and injected at a titer of 2.5×10^{13}GC/ml.

In vivo phrenic nerve recording

In vivo recording preparation: ChR2$^+$ mice were initially anesthetized with urethane (1.5 g/kg body weight, intraperitoneal injection), Supplementary injections of 0.2g/kg urethane were administered as needed by assessing any withdrawal reflex or changes in heart rate or respiration rate in response to a noxious paw pinch. A femoral vein was catheterized for intravenous drug delivery, mice were tracheotomized, bilaterally vagotomized in the neck and mechanically ventilated with 50% O_2, balance N_2 (70–90 breaths/min; tidal volume 0.5ml). The initial ventilator frequency was set so that animals were near their apneic threshold. CO_2 was then added to the inspired port of the ventilator to raise end-tidal CO_2 2–4 mmHg above the apneic threshold. Paralysis was instituted with succinyl choline chloride (2mg /kg, I.V.) and maintained with an intravenous infusion (0.5ml/hr) of lactated Ringer solution containing succinylcholine chloride (10mg/ml). Expired CO_2 was continuously

measured with an infrared analyzer (CWE Incorporated) and maintained constant by adjusting the CO_2 added to the inspired gas. Rectal temperature was monitored and maintained at 37.5–38.5°C by means of a thermistor-controlled heating pad and heat lamp. Transcutaneous needle electrodes were placed over the caudal ribcage to record ECG and respiratory EMG as a marker of the inspiratory phase of breathing. Mice were placed in a stereotaxic head holder. As previously described for rats (Monnier et al., 2003), a midline incision was made in the dorsal aspect of the neck, the underlying muscles separated, a small amount of the caudal aspect of the occipital bone removed and the dura and arachnoid membranes removed to expose the dorsal surface of the brainstem at the level of the area postrema. The calamus was used as the reference point and was defined as the caudal pole of area postrema (see Figure S1B) The right phrenic nerve was isolated using a dorsal approach in the neck, placed on a bipolar silver wire electrode and bathed in mineral oil for recording respiratory motor activity. Phrenic nerve activity was amplified, filtered (band pass 0.3–10kHz), full-wave rectified, and integrated (Paynter filter; time constant 15ms).

Optogenetic stimulation: For optogenetic stimulation we used a 200 μm diameter optic fiber (Plexon Optical Patch cable). The stimulus was generated by an LED Driver (PlexBright LD-1 Single Channel LED Driver, 473nm) connected to a blue LED module (PlexBright LED 465nm). Duration and frequency of light pulses were generated by a Master-8 stimulator (A.M.P.I.). The power output was measured at the tip of the optical fiber with a light meter (PM1000USB, ThorLabs) and preset at 4mW/mm^2 before each experiment. The fiber was positioned on the dorsal surface of the medulla 200–400 μm lateral to the midline, and ± 600 μm rostrocaudal to the calamus. The LED stimulation was delivered at an intensity of 4mW/mm^2 using 10ms pulses at 20Hz for 1min trains. A total of 5–6 trains separated by 4min were delivered. At the end of the experiment, the location of the fiber was marked for subsequent histological confirmation of the stimulating site by driving the fiber several hundred μm into the brainstem.

Leptin injections: For leptin injections into the NTS of NALCN-cKO mice a single barrel micropipette (10–15 μm o.d.) containing leptin (2μM in PBS, pH 7.4) was positioned 200–400 μm lateral to the midline and ± 200 μm rostrocaudal to calamus (i.e., a similar region to that explored *ex vivo*).The pipette was connected to a pressure source via a solenoid valve, advanced 200 μm ventral to the dorsal surface and 30nL of leptin injected within 10–30sec. Injection volumes were directly monitored using a compound microscope equipped with a fine reticule.

Termination: Experiments were terminated one hour after either the optogenetic stimulation or injection of leptin by administering supplemental urethane (0.2ml i.v.). Mice were then perfused transcardially with 4% freshly depolymerized paraformaldehyde (PFA, EM Science) in 0.12M PB. Brains were dissected from the skull and cryoprotected in successive passes of 10, 20, and 30% sucrose in phosphate buffered saline (PBS). Cryoprotected brains were sectioned serially at 50 μm in coronal plane on a vibrating blade microtome and proceeded to immunostainings. A set of sections were stained with cresyl violet to confirm the stimulation site of the optic fiber.

Ex vivo slice recording

Slice preparation: 4 to 6-weeks-old Halo$^+$ mice or NALCN-cKO mice were anesthetized with isoflurane and euthanized by decapitation. Acute brainstem slices (275μm thickness) were cut using a vibratome (Leica VT 1200S) in ice-chilled low calcium, high magnesium ACSF containing (in mM): 125 NaCl, 25 glucose, 25 $NaHCO_3$, 2.5 KCl, 1.25 NaH_2PO_4, 0.5 $CaCl_2$, and 7 $MgCl_2$, equilibrated with 95% O_2 and 5% CO_2 (pH 7.4). Slices were then transferred to a 34°C pre-warmed chamber filled with ACSF containing (in mM): 125 NaCl, 25 glucose, 25 $NaHCO_3$, 2.5 KCl, 1.25 NaH_2PO_4, 2 $CaCl_2$, and 1 $MgCl_2$ equilibrated with 95% O_2 and 5% CO_2.

Data acquisition: Slices were visualized using an Olympus upright microscope using oblique infrared illumination and a water-immersion 40X objective connected to a video camera (Q-imaging). Patch-clamp recordings were performed with an Axopatch-200B amplifier controlled by pClamp 10.3 software using a Digidata 1440A digitizer (Axon). For voltage-clamp and current clamp recordings, signals were filtered at 2–5KHz and digitized at 10–20kHz. Traces presented in the figures represent single sweeps (current clamp recordings) or the average of up to 5 sweeps (voltage clamp recordings).

Whole-cell patch-clamp recordings: Pipettes were pulled from borosilicate glass capillaries (Sutter; OD 1.5mm, ID 0.86mm) using a horizontal puller (P97, Sutter). Tip resistances in working solutions ranged from 3 to 5MΩ yielding series resistances of 10 to 15MΩ. Series resistance was not compensated. All recordings were carried out at a bath temperature of 28–30°C. For current clamp recordings, glass pipettes were filled with a potassium-based solution containing (in mM): 140 K-gluconate, 8 NaCl, 2 $MgCl_2$, 0.1 EGTA, 10 HEPES, 2 Mg-ATP, and 0.2 Na_3-GTP (pH 7.3 with KOH). The bath solution (ACSF) contained (in mM): 125 NaCl, 25 glucose, 25 $NaHCO_3$, 2.5 KCl, 1.25 NaH_2PO_4, 2 $CaCl_2$, 1 $MgCl_2$, 3 kynurenic acid, 0.1 picrotoxin, and 0.001 strychnine. For voltage-clamp ramp recordings, we used a cesium-based internal solution composed of (in mM): 138 $CsMeSO_4$, 8 NaCl, 2 $MgCl_2$, 10 EGTA, 10 HEPES, 2 Mg-ATP, 0.2 Na_3-GTP, and 5 Qx-314 (pH 7.3 with CsOH). For these recordings, the extracellular ACSF also contained (in mM): 1 CsCl, 0.01 nimodipine, 0.001 TTX, 0.5 $BaCl_3$, 3 kynurenic acid, 0.1 picrotoxin (Tocris), and 0.001 strychnine.

Perforated patch-clamp recordings—The protocol of Heigele and colleagues was adapted (Heigele et al., 2016). Fresh gramicidin stock solution (20mg/ml in DMSO) was prepared daily. 2.5μl of stock solution were added to 1ml of warm (35°C) K-gluconate based internal solution (final concentration: 50 μg/ml). The solution was then vortexed for 1min, sonicated for 15min and finally filtered using a 0.2μm filter. Pipettes were pulled from borosilicate glass capillaries (Sutter; OD 1.5mm, ID 0.86mm) using a horizontal puller (p97, Sutter). Recording pipettes with resistances of 4–5 MΩ were tip-filled with gramicidin-free K-gluconate solution and then back-filled with the gramicidin K-gluconate solution. Upon formation of a gigaseal, access resistance was monitored in voltage clamp every 15 s until it reached 80–150MOhm. 0.1% lucifer yellow was included in the back-filled internal solution to visually confirm in real time the integrity of the membrane. If any lucifer yellow staining of the cell body was observed after completion of the recordings, data were discarded. All

perforated patch recordings were performed at 28–30°C in the presence of 3mM kynurenic acid, 0.1M picrotoxin, and 0.001M strychnine.

Drug application—Fresh stock solution of leptin (1mg/ml) was prepared in PBS (pH 8.0) and the leptin working solution was diluted in ACSF fresh from stock on the day of use. Leptin (200nM) was focally applied through a glass pipette with an N_2-powered dispenser (Picospritzer 2, General Valve). For gadolinium experiments, $GdCl_3$ (10 μM) was added to the extracellular solution. For $NMDG^+$ substitution experiments, the extracellular solution contained: 125 NMDG, 25 glucose, 25 $NaHCO_3$, 2.5 KCl, 1.25 NaH_2PO_4, 1 $CaCl_2$, and 2 $MgCl_2$, equilibrated with 95% O_2 and 5% CO_2 (pH 7.4).

Single-cell patch RNA sequencing

Single-cell sample collection: Single cell samples were collected from $Halo^+$ mice of both sexes. Glass pipettes were sterilized in a drying oven at 200°C overnight or cleaned with RNase zap. All electrophysiology devices were cleaned with RNase Zap (AM9780, Invitrogen). The internal solution contained (in mM): 140 K-gluconate, 8 NaCl, $2MgCl_2$, 0.1 EGTA, 10 HEPES, 2 Mg-ATP, 0.2 Na_3-GTP, and 1U/μl RNase inhibitor (pH 7.3). Pipettes were filled with 4–6μl of the solution using RNase-free microloader tip pipettes. LepRb neurons were identified by expression of YFP. After recording the neuronal firing pattern, the cytoplasm and nucleus were harvested by applying a gentle negative pressure; the suction process was monitored using the infra-red DIC camera (40x-lens). After aspiration, pressure was released, and the pipette was slowly withdrawn from the cell to form an outside-out patch. The pipette was quickly removed and placed on a custom-built holder where a 7x stereoscope guided the tip of the pipette to the bottom of a 0.2ml RNase-free tube containing RNase-free lysis buffer. The tip was gently broken, and the content expelled using positive pressure. Samples were kept in room temperature for 5 min (lysis) and then stored at −80°C.

cDNA library preparation and sequencing: The Northwestern University sequencing core (NUseq) prepared the cDNA using the SMART-Seq v4 Ultra Low Input RNA Kit for Sequencing Kit (Takara) and quality check was performed using a bioanalyzer (Agilent). Cell samples with similar size distributions were chosen for cDNA library preparation using the Nextera XT DNA library prep kit (Illumina).

In situ hybridization histochemistry (ISHH; RNAscope)

Section preparation: Mice were deeply anesthetized with sodium pentobarbital (Euthasol®, 150 mg/kg, i.p.) and transcardially perfused with 4% PFA in 0.12 M PB. Brains were post-fixed in the same solution overnight, and cryoprotected in 30% sucrose in PBS with 0.1% diethyl pyrocarbonate (DEPC). Coronal sections (14 μm) were cut using a freezing stage microtome and mounted on positively charged glass slides (Superfrost plus, 12-550-15, Fisher). A total of at least 168 coronal serial sections were cut from each brain along the rostral-caudal axis of the medulla; according to the Paxinos and Franklin's Mouse Brain stereotaxic atlas (Franklin and Paxinos, 2019). The NTS lay between −8.15 and −6.59mm from Bregma. Twenty-eight sections spaced 84 μm apart from each other and

corresponding to the caudal and rostral parts of the NTS were used for ISHH. Sections were stored in DEPC treated PBS.

Probe hybridization: ISHH was performed using a single (RNAscope 2.5 High Definition BROWN Assay kit; ACD Biotechne) or duplex probe assay kit (RNAscope 2.5 Duplex Assay kit) and probes from Advanced Cell Diagnostics (Newark, CA) following the manufacturer's user manual with minor modifications. Briefly, sections were first treated with 0.9% H_2O_2 and 10% methanol in PBS for 10min and then with 9.86mM sodium citrate buffer solution (pH 6.0) for 2min at 91°C. Sections were next treated with proteinase K (1 μg/ml) for 15min at 40°C. Then probes (see Key Resources Table) were hybridized to sections for 2hr at 40°C. Signals were amplified using the single or duplex probe assay kit reagents. Before the first amplification step, sections were washed in 0.1x saline sodium-citrate (SSC) buffer at 33°C. Sections were also washed in the same solution after each of the following 6 amplification steps; the first three times at 33°C, and then at room temperature. For single assay, C1-probe signal was detected using DAB (3,3′-diaminobenzidine; brown). For duplex assay, C1-probe signal was detected with SG (SG substrate kit peroxidase; blue; Vector Laboratories) and the C2-probe signal was detected with fast-red, respectively. Cells were counter-stained using 25% methyl green solution and coverslipped with Vectamount (Vector Laboratories). Sections that were further processed for immunostaining were not coverslipped but immediately processed for immunostaining (see below).

Immunohistology

Section preparation: Mice were deeply anesthetized with sodium pentobarbital (Euthasol®, 150mg/kg i.p.) and perfused with 4% PFA in 0.12M PB; brains were dissected and stored in 30% sucrose in PBS at 4°C. Serial coronal or sagittal brain sections were collected using a freezing microtome and the sections were stored in PBS with 0.0008% sodium azide at 4°C.

Fluorescence immunostaining: Free-floating sections (14μm) were incubated for 1-hour in blocking solution containing: 3% normal goat serum (NGS; GIBCO), 1% bovine serum albumin (BSA, Fisher), 0.5% Triton X-100, and 0.5% dimethyl sulfoxide (DMSO) in Tris-buffered saline (TBS, 0.1M Tris-HCl/0.15M NaCl). Sections were then incubated with primary antibodies diluted in TBS containing 1% NGS, 1%BSA, and 0.2% Triton x-100 for 24–72hrs at 4°C. Sections were washed 4X with TBS, then incubated with Alexa-conjugated secondary antibodies diluted in TBS buffer containing 1% NGS, 1%BSA, and 0.2% Triton x-100 for 1hr. Sections were washed overnight at 4°C, mounted, and coverslipped with Mowiol. Sections processed without primary antibody incubation were free of specific immunoreaction products (not shown).

Brightfield immunostaining for cFos and pSTAT3 visualization. Free-floating sections (30 μm) were pretreated with a mixture containing, DMSO, 30% H_2O_2, and methanol at 1:1:4 ratio for 20min. Sections were triple rinsed with TBS and incubated for 1hr in blocking solution. Next, sections were incubated with primary antibodies diluted in solution containing 1% NGS, 1%BSA, and 0.2% Triton x-100 in TBS for 24–48hrs at 4°C. Sections

were washed 4X with TBS, then incubated with biotinylated-secondary antibodies diluted in TBS buffer containing 1% NGS, 1%BSA, and 0.2% Triton x-100 for 1hr. Sections were washed four times with TBS and incubated with solution containing 1% NGS, 1%BSA, 0.2% Triton x-100, and avidin-biotin complex (ABC kit, Vector Labs). The bound antibodies were visualized using DAB as a substrate. The sections were coverslipped with Entellan (EM Science).

Brightfield immunostaining after ISHH labeling: ISHH-labeled sections adhered to glass slides were treated for 1hr in TBS containing 3% NGS, 1% BSA, 0.2% Triton X-100 and then incubated overnight with primary antibodies diluted in TBS containing 1% NGS, 1% BSA, and 0.2% Triton x-100 at 4°C. The bound antibodies were visualized by the ABC method using SG Substrate. Information for primary and secondary antibodies are provided in the Key Resources table.

Image acquisition: Confocal fluorescent images were taken with a Zeiss LSM 510 Meta Inverted Confocal Microscope system. Z stack images were acquired with 1 μm thick optical planes. Images were analyzed individually or in z stacks of different depths. For colocalization experiments, Zeiss immersion oil 518F was used with a 63x plan-apochromatic lens (numerical aperture 1.6). Bright field images were acquired with a Spot RT CCD video camera (Diagnostic Instruments) mounted on a Nikon Eclipse E800 microscope. All images were processed with Adobe Photoshop CC or Adobe Illustrator CC. Brightness and contrast were adjusted.

Reagents: Unless otherwise reported, all reagents were purchased from Millipore-Sigma. Antibodies used in this study are listed in the Key Resources table.

Plethysmography

Body temperature measurements: Temperature transponders (IPTT-300) were inserted subcutaneously in mice 1 week before plethysmography experiments. Mice were anesthetized with isoflurane (2%) and transponders were injected underneath the skin of the dorsal right side of the body. The skin opening was closed with vetbond. During plethysmography, body temperatures were measured every minute during baseline and gas challenge measurements in the plethysmography chamber using a DAS-8007 Wireless Reader.

Acclimatization: Breathing in awake, unrestrained mice was evaluated with whole-body flow-plethysmography (DSI). Breathing parameters, such as tidal volume, frequency, and minute ventilation, were acquired with the FinePointe software (DSI). The room air bias flow rate was set at 500mL/min. All plethysmography experiments were done during the light phase between ZT3 and ZT9. Mice were first acclimatized to the chambers for at least 2 consecutive days, 1hr each day, to decrease anxiety and exploratory behaviors. Animals met the criteria of acclimatization when they settled quietly and awake within 20min of placement in chambers.

Baseline breathing and gas challenges: On the test day, mice were placed in the plethysmography chambers for a 20min acclimatization period before recording a 10min breathing baseline in room air. Mice were then exposed to gas containing either 5% CO_2 (in 21% O_2, balance N_2), or 10% O_2 (in 90% N_2) for 10min. Each gas exposure was followed by a 7min recovery period in room air. All sessions were video recorded with a video camera.

High fat diet feeding: After lean mice completed testing for baseline breathing and chemosensitivity, they were fed an *ad libitum* high-fat diet (HFD, 60% calories from fat, cat. #S3282 Bio-Serve) for 3 weeks. Body weight was measured at least twice/week and breathing was measured after the first and third week of HFD.

Mouse leptin assay

Blood sample collection: Blood samples were collected in the morning, 3hrs post the onset of the light cycle. Body weights were measured, and blood samples were drawn by puncturing the submandibular vein with a sterile lancet (5mm). From each animal, ~100μl blood was collected in ice-chilled K-EDTA pretreated tubes (Microvette, SARSTEDT). To collect plasma, samples were centrifuged for 5min at 2000rpm, 4°C. The supernatant was stored at −80°C until further use. Blood samples were taken each week at the same time of day before and during high fat diet feeding.

Leptin ELISA assay: Leptin ELISA assay measurements were performed by the Comprehensive Metabolic Core at Northwestern University. Leptin concentration in plasma samples from lean (not diluted) and HFD fed cohort (1:6 dilution) were measured using the mouse leptin ELISA kit (Crystal Chem).

Viral delivery

Stereotaxic surgery: 3 to 5-months-old LepRb-Cre mice of both sexes, were anesthetized with isoflurane inhalation (4%) and secured in a stereotaxic frame (David Kopf Instruments). Isoflurane concentration was reduced to 2% with a flow rate of 0.8L/min. The head of the animals was tilted nose down by ~10 degrees. Hair was removed with Nair and the skin was cleaned with alcohol and iodine. Eye ointment was applied to the eyes to prevent dryness. Under magnification, a midline incision was made over the dorsal surface of the neck. Neck muscles were carefully retracted, the anterior atlanto-occipital membrane incised, and the dura removed. The calamus served as a reference point for injection.

Viral delivery: Injections were performed using a 35G blunt-end Nanofil syringe (1uL). Points of entry to target the NTS were −0.2mm to calamus; ± 0.1mm lateral to the midline; 0.4mm ventral to the surface of the brainstem. The syringe was inserted into the brainstem at a 35 degree angle (from anterior to posterior). A volume of 150nL of virus/side was delivered bilaterally at a rate of 0.15ml/min. The syringe remained in place for a minimum of 5min after each injection. After 5min, the needle was retracted, the muscles were sutured with sterile polyglactin suture (6–0) and the skin incision was closed with sterile monofilament suture (4–0) and Vetbond (3M).

Post-operative care: Analgesics (single s.c. injection of 1 mg/kg, Buprenorphine SR; daily s.c. injection of 1 mg/kg, Meloxicam for up to three days) were administered post-operatively. Following a minimum 21-day recovery period, mice were sacrificed for anatomical tracing studies.

QUANTIFICATION AND STATISTICAL ANALYSIS

Data reported in the text and figures represent mean ± SEM. For statistical comparison, GraphPad Prism5 was used. Sample sizes, error bars, statistical tests and significance levels are provided in each figure legend.

Phrenic nerve recording—Data acquisition and analyses were done using Spike2 (CED). For analysis, 30sec of data were collected every 2min for leptin administration experiments and every 5min for LED stimulation. Two animals were excluded from optogenetic experimental analysis due to diminishing health conditions during recording. One wild-type animal in leptin injection experiments was excluded from data analysis due to an invalid injection site. Data obtained during control measurements and for 1hr following leptin administration were analyzed using a nested analysis of variance model with group as the between-mice factor and time as the within mice factor. The effect of light stimulation versus control, or NALCN-cKO versus control on phrenic motor activity was compared using a two-way ANOVA with main factors of treatment (light stimulation or genotype) and time. Significant differences were followed up using the Bonferroni procedure for multiple comparisons. P values < 0.05 are indicated in figures by*.

Slice electrophysiology—For data analysis we used Clampfit10.2 and MATLAB. The input resistance of the cells was calculated in current clamp from the slope of the voltage responses measured at the end of two hyperpolarizing current injections (−100 and −200pA, 2sec). Voltage values were averaged over a 100ms time window and divided by the difference in amplitude of the current pulses. Cells were held at −60mV and single action potentials were evoked by a 5 or 7ms current pulse injection (100pA, 10 sweeps). To compare the properties of single action potentials between cell types, action potential sweeps were aligned by their peaks and then averaged. To determine thresholds, we calculated the first derivative of the membrane potential and took the value that crosses 0 immediately before the peak of the action potential. Action potential frequency was obtained by counting the number of action potentials during 2sec depolarizing pulse steps. The inter-spike interval (ISI) ratio was calculated by dividing the duration of the ISI between the first two spikes by that between the last two spikes during a 2sec long 100pA depolarizing step. Slow voltage ramps (from −60 to +20 mV, 1sec) were used to measure the leptin-evoked current, which was obtained by subtracting offline the current recorded in control conditions from that in the presence of leptin. The reversal potential was obtained by linear fit of the subtracted current.

Single-cell patch RNA sequencing—Quantification and statistical analysis were provided by the NU sequencing core.

In situ hybridization

Data quantification: The region of the NTS was defined using the Paxinos mouse brain atlas. We used calamus (caudal end of the area postrema) as the reference point 0. We counted four sections caudal and three sections rostral to the reference point each distanced 84 μm along the rostral-caudal axis. From each section, an image from each side of the NTS was acquired with a 40x plan-fluor lens (numerical aperture 1.3) using Spot RT CCD video camera (Diagnostic Instruments) mounted on a Nikon Eclipse E800 microscope. Counting was performed under visual guidance using a 60x plan-apochromatic lens (numerical aperture 1.4) in the acquired images. LepRb NTS neurons were identified and quantified by FastRed LepRb mRNA puncta in methyl green counterstained cells.

For duplex ISHH assays, we first counted cells containing FastRed LepRb mRNA puncta. Then cells that co-expressed SG substrate labeled Galanin, GLP-1, CCK, or POMC mRNA with LepRb mRNA were counted. Data was expressed as percentage of number of co-expressing cells/LepRb mRNA cells.

Plethysmography

Behavioral scoring: All sessions were video recorded and analyzed by a person who was blinded to the mouse genotype. Behavior was scored into one of four categories: quiet awake, sleep (eyes closed), grooming, exploring. Breathing segments categorized as quiet awake were analyzed.

Data analysis—We used the FinePointe software (DSI) to identify airflow waveforms, minute ventilation ($\dot{V}_E$), tidal volume (V_T) and breathing frequency (f), where $\dot{V}_E = V_T \times f$. To identify apneas and breathing irregularity, we used custom written MATLAB code to detect the peaks of inspiratory airflow. Inter-breath interval (IBI) irregularity and apnea analyses were adapted from van der Heijden and Zoghbi (2018). IBI was defined as the duration from one peak to the next peak. A spontaneous apnea was defined as an IBI > 0.5sec and at least twice the length of the average of the six surrounding breaths (three previous and three following). Apneas either immediately preceding or following a sigh were excluded from analysis. IBI irregularity was defined as: IBI irregularity = abs (breath length$_{(n+1)}$-breath length$_{(n)}$)/breath length$_{(n)}$. Breathing during the initial 3min of a gas challenge was not included in this analysis as exploratory behavior confounded the analysis. In the Poincare analysis, short-term variability (SD1) expressed the variability in time from one breath interval to the next breath interval. Long-term variability (SD2) quantified the overall variability in breath intervals across the recording session. SD1 and SD2 were calculated as described by Karmakar et al., 2013. SDRR is the standard deviation of the IBIs. SDSD is the standard deviation of the successive differences of the IBIs. Successive differences, the R-R intervals, were defined as $RR_i = IBI_{i+1} - IBI_i$. The following equations were used to calculate the values:

$$SDSD = \sqrt{\frac{1}{N}\sum_{i=1}^{N}(RR_i - \overline{RR})^2}$$

$$SDRR = \sqrt{\overline{IBI^2} - \overline{IBI^2}}$$

$$SD1 = \frac{1}{\sqrt{2}} \times SDSD$$

$$SD2 = \sqrt{2SDRR^2 - (1/2)SDSD^2}$$

Supplementary Material

Refer to Web version on PubMed Central for supplementary material.

ACKNOWLEDGMENTS

This work was supported by National Institutes of Health (NIH) grants HL122921 (D.R.M.) and NS 090346 (M.M.). J.D. was also supported by the General Motor Control Mechanisms and Disease Training Program (T32NS041234). In addition, this work was supported by the Comprehensive Metabolic Core at Northwestern University and the Northwestern University Sequencing Core (NUSeq). We thank Dr. Tony Kowal and Mr. Mahmoud Farhan for their help in maintaining and genotyping the various transgenic mouse colonies.

REFERENCES

Baertsch NA, Baertsch HC, and Ramirez JM (2018). The interdependence of excitation and inhibition for the control of dynamic breathing rhythms. Nat. Commun 9, 843. [PubMed: 29483589]

Bassi M, Giusti H, Leite CM, Anselmo-Franci JA, do Carmo JM, da Silva AA, Hall JE, Colombari E, and Glass ML (2012). Central leptin replacement enhances chemorespiratory responses in leptin-deficient mice independent of changes in body weight. Pflugers Arch. 464, 145–153. [PubMed: 22585210]

Bassi M, Furuya WI, Menani JV, Colombari DS, do Carmo JM, da Silva AA, Hall JE, Moreira TS, Wenker IC, Mulkey DK, and Colombari E (2014). Leptin into the ventrolateral medulla facilitates chemorespiratory response in leptin-deficient (ob/ob) mice. Acta Physiol. (Oxf.) 211, 240–248. [PubMed: 24521430]

Bassi M, Nakamura NB, Furuya WI, Colombari DS, Menani JV, do Carmo JM, da Silva AA, Hall JE, and Colombari E (2015). Activation of the brain melanocortin system is required for leptin-induced modulation of chemorespiratory function. Acta Physiol. (Oxf.) 213, 893–901. [PubMed: 25207799]

Bassi M, Furuya WI, Zoccal DB, Menani JV, Colombari DS, Mulkey DK, and Colombari E (2016). Facilitation of breathing by leptin effects in the central nervous system. J. Physiol 594, 1617–1625. [PubMed: 26095748]

Baver SB, Hope K, Guyot S, Bjørbaek C, Kaczorowski C, and O'Connell KM (2014). Leptin modulates the intrinsic excitability of AgRP/NPY neurons in the arcuate nucleus of the hypothalamus. J. Neurosci 34, 5486–5496. [PubMed: 24741039]

Burki NK, and Baker RW (1984). Ventilatory regulation in eucapnic morbid obesity. Am. Rev. Respir. Dis 129, 538–543. [PubMed: 6424520]

Caballero-Eraso C, Shin MK, Pho H, Kim LJ, Pichard LE, Wu ZJ, Gu C, Berger S, Pham L, Yeung HB, et al. (2019). Leptin acts in the carotid bodies to increase minute ventilation during wakefulness and sleep and augment the hypoxic ventilatory response. J. Physiol 597, 151–172. [PubMed: 30285278]

Campo A, Frühbeck G, Zulueta JJ, Iriarte J, Seijo LM, Alcaide AB, Galdiz JB, and Salvador J (2007). Hyperleptinaemia, respiratory drive and hypercapnic response in obese patients. Eur. Respir. J 30, 223–231. [PubMed: 17459895]

Chang Z, Ballou E, Jiao W, McKenna KE, Morrison SF, and McCrimmon DR (2013). Systemic leptin produces a long-lasting increase in respiratory motor output in rats. Front. Physiol 4, 16. [PubMed: 23408476]

Chlif M, Keochkerian D, Choquet D, Vaidie A, and Ahmaidi S (2009). Effects of obesity on breathing pattern, ventilatory neural drive and mechanics. Respir. Physiol. Neurobiol 168, 198–202. [PubMed: 19559105]

Del Negro CA, Funk GD, and Feldman JL (2018). Breathing matters. Nat. Rev. Neurosci 19, 351–367. [PubMed: 29740175]

Dempsey JA, Mitchell GS, and Smith CA (1984). Exercise and chemoreception. Am. Rev. Respir. Dis 129, S31–S34. [PubMed: 6421215]

Dempsey JA, Blain GM, and Amann M (2014). Are type III-IV muscle afferents required for a normal steady-state exercise hyperpnoea in humans? J. Physiol 592, 463–474. [PubMed: 24000177]

Dhar M, Wayman GA, Zhu M, Lambert TJ, Davare MA, and Appleyard SM (2014). Leptin-induced spine formation requires TrpC channels and the CaM kinase cascade in the hippocampus. J. Neurosci 34, 10022–10033. [PubMed: 25057204]

Donovan LM, and Kapur VK (2016). Prevalence and characteristics of central compared to obstructive sleep apnea: analyses from the sleep heart health study cohort. Sleep (Basel) 39, 1353–1359.

Eckert DJ, Jordan AS, Merchia P, and Malhotra A (2007). Central sleep apnea: pathophysiology and treatment. Chest 131, 595–607. [PubMed: 17296668]

Elias CF, Kelly JF, Lee CE, Ahima RS, Drucker DJ, Saper CB, and Elmquist JK (2000). Chemical characterization of leptin-activated neurons in the rat brain. J. Comp. Neurol 423, 261–281. [PubMed: 10867658]

Fields DP, and Mitchell GS (2015). Spinal metaplasticity in respiratory motor control. Front. Neural Circuits 9, 2. [PubMed: 25717292]

Flourakis M, Kula-Eversole E, Hutchison AL, Han TH, Aranda K, Moose DL, White KP, Dinner AR, Lear BC, Ren D, et al. (2015). A conserved bicycle model for circadian clock control of membrane excitability. Cell 162, 836–848. [PubMed: 26276633]

Ford NC, Ren D, and Baccei ML (2018). NALCN channels enhance the intrinsic excitability of spinal projection neurons. Pain 159, 1719–1730. [PubMed: 29746349]

Framnes SN, and Arble DM (2018). The bidirectional relationship between obstructive sleep apnea and metabolic disease. Front. Endocrinol. (Lausanne) 9, 440. [PubMed: 30127766]

Franklin K, and Paxinos G (2019). Paxinos and Franklin's Mouse Brain Stereotaxic Atals Coordinates, 5th Edition (Academic Press).

Friedman JM (2019). Leptin and the endocrine control of energy balance. Nat. Metab 1, 754–764. [PubMed: 32694767]

Fu C, Xue J, Wang R, Chen J, Ma L, Liu Y, Wang X, Guo F, Zhang Y, Zhang X, and Wang S (2017). Chemosensitive Phox2b-expressing neurons are crucial for hypercapnic ventilatory response in the nucleus tractus solitarius. J. Physiol 595, 4973–4989. [PubMed: 28488367]

Fukushi I, Yokota S, and Okada Y (2019). The role of the hypothalamus in modulation of respiration. Respir. Physiol. Neurobiol 265, 172–179. [PubMed: 30009993]

Garfield AS, Patterson C, Skora S, Gribble FM, Reimann F, Evans ML, Myers MG Jr., and Heisler LK (2012). Neurochemical characterization of body weight-regulating leptin receptor neurons in the nucleus of the solitary tract. Endocrinology 153, 4600–4607. [PubMed: 22869346]

Gavello D, Carbone E, and Carabelli V (2016). Leptin-mediated ion channel regulation: PI3K pathways, physiological role, and therapeutic potential. Channels (Austin) 10, 282–296. [PubMed: 27018500]

Hayashi F, Coles SK, Bach KB, Mitchell GS, and McCrimmon DR (1993). Time-dependent phrenic nerve responses to carotid afferent activation: intact vs. decerebellate rats. Am. J. Physiol 265, R811–R819. [PubMed: 8238451]

Hayes MR, Skibicka KP, Leichner TM, Guarnieri DJ, DiLeone RJ, Bence KK, and Grill HJ (2010). Endogenous leptin signaling in the caudal nucleus tractus solitarius and area postrema is required for energy balance regulation. Cell Metab. 11, 77–83. [PubMed: 20074530]

Heida NM, Leifheit-Nestler M, Schroeter MR, Müller JP, Cheng IF, Henkel S, Limbourg A, Limbourg FP, Alves F, Quigley JP, et al. (2010). Leptin enhances the potency of circulating angiogenic cells

via src kinase and integrin (alpha)vbeta5: implications for angiogenesis in human obesity. Arterioscler. Thromb. Vasc. Biol 30, 200–206. [PubMed: 19910644]

Heigele S, Sultan S, Toni N, and Bischofberger J (2016). Bidirectional GABAergic control of action potential firing in newborn hippocampal granule cells. Nat. Neurosci 19, 263–270. [PubMed: 26752162]

Hisadome K, Reimann F, Gribble FM, and Trapp S (2010). Leptin directly depolarizes preproglucagon neurons in the nucleus tractus solitarius: electrical properties of glucagon-like Peptide 1 neurons. Diabetes 59, 1890–1898. [PubMed: 20522593]

Huda R, Pollema-Mays SL, Chang Z, Alheid GF, McCrimmon DR, and Martina M (2012). Acid-sensing ion channels contribute to chemosensitivity of breathing-related neurons of the nucleus of the solitary tract. J. Physiol 590, 4761–4775. [PubMed: 22890703]

Huo L, Grill HJ, and Bjørbaek C (2006). Divergent regulation of proopiomelanocortin neurons by leptin in the nucleus of the solitary tract and in the arcuate hypothalamic nucleus. Diabetes 55, 567–573. [PubMed: 16505217]

Huo L, Maeng L, Bjørbaek C, and Grill HJ (2007). Leptin and the control of food intake: neurons in the nucleus of the solitary tract are activated by both gastric distension and leptin. Endocrinology 148, 2189–2197. [PubMed: 17317774]

Inyushkin AN, Inyushkina EM, and Merkulova NA (2009). Respiratory responses to microinjections of leptin into the solitary tract nucleus. Neurosci. Behav. Physiol 39, 231–240. [PubMed: 19234801]

Inyushkina EM, Merkulova NA, and Inyushkin AN (2010). Mechanisms of the respiratory activity of leptin at the level of the solitary tract nucleus. Neurosci. Behav. Physiol 40, 707–713. [PubMed: 20635220]

Jiang L, Li Z, and Rui L (2008). Leptin stimulates both JAK2-dependent and JAK2-independent signaling pathways. J. Biol. Chem 283, 28066–28073. [PubMed: 18718905]

Kang BJ, Chang DA, Mackay DD, West GH, Moreira TS, Takakura AC, Gwilt JM, Guyenet PG, and Stornetta RL (2007). Central nervous system distribution of the transcription factor Phox2b in the adult rat. J. Comp. Neurol 503, 627–641. [PubMed: 17559094]

Khandoker AH, Karmakar C, Brennan M, Palaniswami M, and Voss A (2013). Poincaré Plot Methods for Heart Rate Variability Analysis (Springer).

Krashes MJ, Koda S, Ye C, Rogan SC, Adams AC, Cusher DS, Maratos-Flier E, Roth BL, and Lowell BB (2011). Rapid, reversible activation of AgRP neurons drives feeding behavior in mice. J. Clin. Invest 121, 1424–1428. [PubMed: 21364278]

Leech J, Onal E, Aronson R, and Lopata M (1991). Voluntary hyperventilation in obesity hypoventilation. Chest 100, 1334–1338. [PubMed: 1935291]

Lourenço RV (1969). Diaphragm activity in obesity. J. Clin. Invest 48, 1609–1614. [PubMed: 5822573]

Lu B, Su Y, Das S, Liu J, Xia J, and Ren D (2007). The neuronal channel NALCN contributes resting sodium permeability and is required for normal respiratory rhythm. Cell 129, 371–383. [PubMed: 17448995]

Lutas A, Lahmann C, Soumillon M, and Yellen G (2016). The leak channel NALCN controls tonic firing and glycolytic sensitivity of substantia nigra pars reticulata neurons. eLife 5, e15271. [PubMed: 27177420]

McDowall LM, Horiuchi J, and Dampney RA (2007). Effects of disinhibition of neurons in the dorsomedial hypothalamus on central respiratory drive. Am. J. Physiol. Regul. Integr. Comp. Physiol 293, R1728–R1735. [PubMed: 17715179]

Messenger SA, and Ciriello J (2013). Effects of intermittent hypoxia on leptin signalling in the carotid body. Neuroscience 232, 216–225. [PubMed: 23201827]

Mokhlesi B (2010). Obesity hypoventilation syndrome: a state-of-the-art review. Respir. Care 55, 1347–1362, discussion 1363–1365. [PubMed: 20875161]

Monnier A, Alheid GF, and McCrimmon DR (2003). Defining ventral medullary respiratory compartments with a glutamate receptor agonist in the rat. J. Physiol 548, 859–874. [PubMed: 12640009]

Moult PR, and Harvey J (2011). NMDA receptor subunit composition determines the polarity of leptin-induced synaptic plasticity. Neuropharmacology 61, 924–936. [PubMed: 21752339]

Myers MG Jr., Münzberg H, Leinninger GM, and Leshan RL (2009). The geometry of leptin action in the brain: more complicated than a simple ARC. Cell Metab. 9, 117–123. [PubMed: 19187770]

Nattie EE (2001). Central chemosensitivity, sleep, and wakefulness. Respir. Physiol 129, 257–268. [PubMed: 11738659]

O'Donnell CP, Schaub CD, Haines AS, Berkowitz DE, Tankersley CG, Schwartz AR, and Smith PL (1999). Leptin prevents respiratory depression in obesity. Am. J. Respir. Crit. Care Med 159, 1477–1484. [PubMed: 10228114]

O'Donnell CP, Tankersley CG, Polotsky VP, Schwartz AR, and Smith PL (2000). Leptin, obesity, and respiratory function. Respir. Physiol 119, 163–170. [PubMed: 10722859]

Pérez SE, Wynick D, Steiner RA, and Mufson EJ (2001). Distribution of galaninergic immunoreactivity in the brain of the mouse. J. Comp. Neurol 434, 158–185. [PubMed: 11331523]

Pho H, Hernandez AB, Arias RS, Leitner EB, Van Kooten S, Kirkness JP, Schneider H, Smith PL, Polotsky VY, and Schwartz AR (2016). The effect of leptin replacement on sleep-disordered breathing in the leptin-deficient ob/ob mouse. J Appl Physiol (1985) 120, 78–86. [PubMed: 26472867]

Piper AJ, and Grunstein RR (2011). Obesity hypoventilation syndrome: mechanisms and management. Am. J. Respir. Crit. Care Med 183, 292–298. [PubMed: 21037018]

Polotsky M, Elsayed-Ahmed AS, Pichard L, Harris CC, Smith PL, Schneider H, Kirkness JP, Polotsky V, and Schwartz AR (2012). Effects of leptin and obesity on the upper airway function. J Appl Physiol (1985) 112, 1637–1643. [PubMed: 22345430]

Porzionato A, Rucinski M, Macchi V, Stecco C, Castagliuolo I, Malendowicz LK, and De Caro R (2011). Expression of leptin and leptin receptor isoforms in the rat and human carotid body. Brain Res. 1385, 56–67. [PubMed: 21334312]

Qiu J, Fang Y, Rønnekleiv OK, and Kelly MJ (2010). Leptin excites proopiomelanocortin neurons via activation of TRPC channels. J. Neurosci 30, 1560–1565. [PubMed: 20107083]

Rakoczy RJ, Pye RL, Fayyad TH, Santin JM, Barr BL, and Wyatt CN (2018). High fat feeding in rats alters respiratory parameters by a mechanism that is unlikely to be mediated by carotid body type I cells. Adv. Exp. Med. Biol 1071, 137–142. [PubMed: 30357744]

Ren D (2011). Sodium leak channels in neuronal excitability and rhythmic behaviors. Neuron 72, 899–911. [PubMed: 22196327]

Shanley LJ, Irving AJ, and Harvey J (2001). Leptin enhances NMDA receptor function and modulates hippocampal synaptic plasticity. J. Neurosci 21, RC186. [PubMed: 11734601]

Shanley LJ, Irving AJ, Rae MG, Ashford ML, and Harvey J (2002). Leptin inhibits rat hippocampal neurons via activation of large conductance calcium-activated K+ channels. Nat. Neurosci 5, 299–300. [PubMed: 11889470]

Shi Y, Abe C, Holloway BB, Shu S, Kumar NN, Weaver JL, Sen J, Perez-Reyes E, Stornetta RL, Guyenet PG, and Bayliss DA (2016). Nalcn is a "leak" sodium channel that regulates excitability of brainstem chemosensory neurons and breathing. J. Neurosci 36, 8174–8187. [PubMed: 27488637]

Spanswick D, Smith MA, Groppi VE, Logan SD, and Ashford ML (1997). Leptin inhibits hypothalamic neurons by activation of ATP-sensitive potassium channels. Nature 390, 521–525. [PubMed: 9394003]

Steier J, Jolley CJ, Seymour J, Roughton M, Polkey MI, and Moxham J (2009). Neural respiratory drive in obesity. Thorax 64, 719–725. [PubMed: 19386586]

Steier J, Lunt A, Hart N, Polkey MI, and Moxham J (2014). Observational study of the effect of obesity on lung volumes. Thorax 69, 752–759. [PubMed: 24736287]

Stein LM, Lhamo R, Cao A, Workinger J, Tinsley I, Doyle RP, Grill HJ, Hermann GE, Rogers RC, and Hayes MR (2020). Dorsal vagal complex and hypothalamic glia differentially respond to leptin and energy balance dysregulation. Transl. Psychiatry 10, 90. [PubMed: 32152264]

Swayne LA, Mezghrani A, Varrault A, Chemin J, Bertrand G, Dalle S, Bourinet E, Lory P, Miller RJ, Nargeot J, and Monteil A (2009). The NALCN ion channel is activated by M3 muscarinic receptors in a pancreatic beta-cell line. EMBO Rep. 10, 873–880. [PubMed: 19575010]

Tankersley C, Kleeberger S, Russ B, Schwartz A, and Smith P (1996). Modified control of breathing in genetically obese (ob/ob) mice. J Appl Physiol (1985) 81, 716–723. [PubMed: 8872638]

van den Top M, Lee K, Whyment AD, Blanks AM, and Spanswick D (2004). Orexigen-sensitive NPY/AgRP pacemaker neurons in the hypothalamic arcuate nucleus. Nat. Neurosci 7, 493–494. [PubMed: 15097991]

van der Heijden ME, and Zoghbi HY (2018). Loss of *Atoh1* from neurons regulating hypoxic and hypercapnic chemoresponses causes neonatal respiratory failure in mice. eLife 7, e38455. [PubMed: 29972353]

Wang H, and Ren D (2009). UNC80 functions as a scaffold for Src kinases in NALCN channel function. Channels (Austin) 3, 161–163. [PubMed: 19535918]

Williams KW, and Smith BN (2006). Rapid inhibition of neural excitability in the nucleus tractus solitarii by leptin: implications for ingestive behaviour. J. Physiol 573, 395–412. [PubMed: 16581866]

Yao Q, Pho H, Kirkness J, Ladenheim EE, Bi S, Moran TH, Fuller DD, Schwartz AR, and Polotsky VY (2016). Localizing effects of leptin on upper airway and respiratory control during sleep. Sleep (Basel) 39, 1097–1106.

Yeh SY, Huang WH, Wang W, Ward CS, Chao ES, Wu Z, Tang B, Tang J, Sun JJ, Esther van der heijden M, et al. (2017). Respiratory network stability and modulatory response to substance P require nalcn. Neuron 94, 294–303.e4. https://pubmed.ncbi.nlm.nih.gov/28392070/. [PubMed: 28392070]

Highlights

- Selective optogenetic activation of LepRb NTS neurons increases tidal volume
- Leptin depolarizes galanin-expressing LepRb NTS neurons by activating NALCN
- NALCN activation in LepRb NTS neurons stimulates breathing in overweight mice
- Failure to activate LepRb NTS neurons may cause hypoventilation in obesity

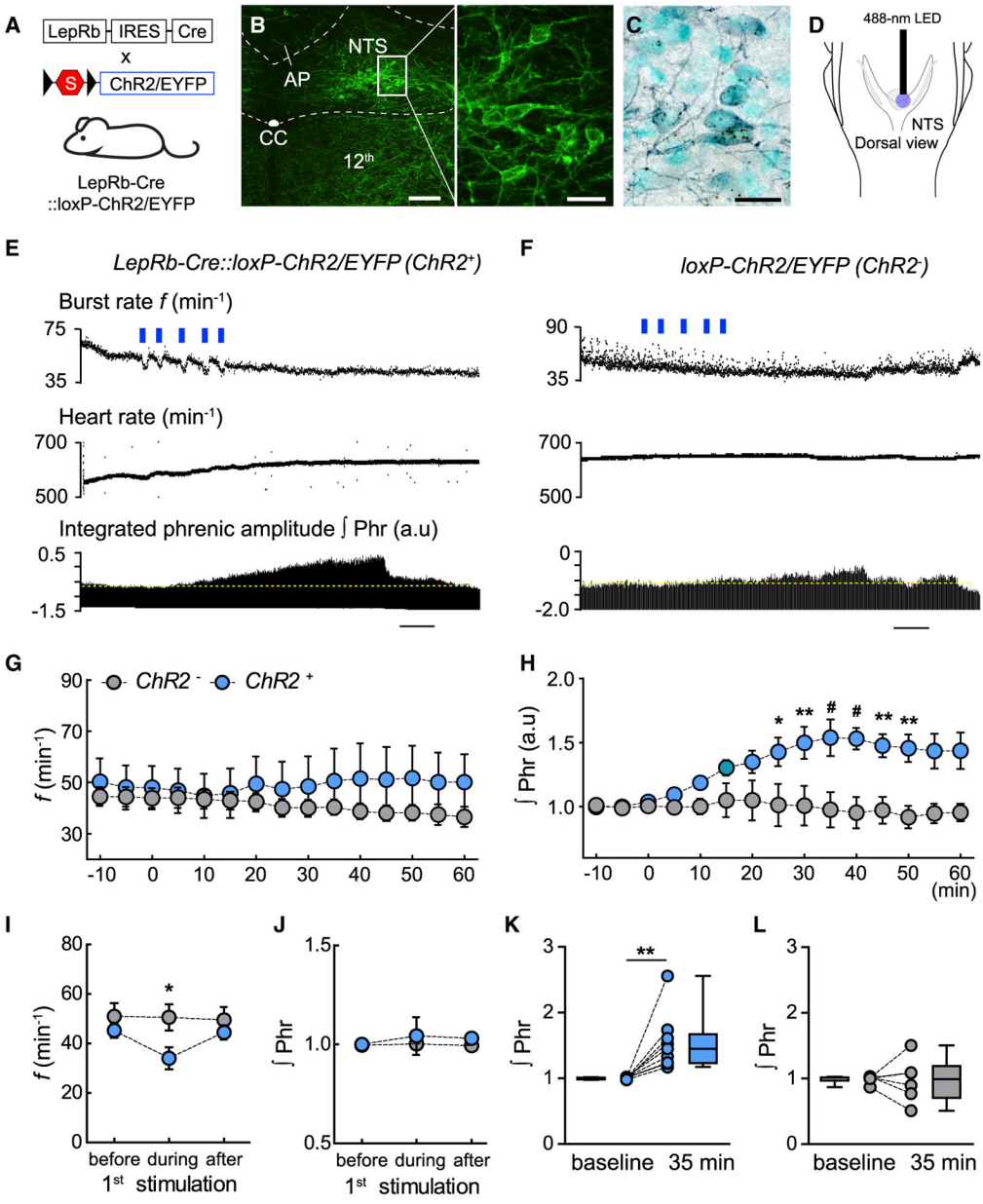

Figure 1. Optogenetic Stimulation of ChR2-Expressing LepRb NTS Neurons Increases Phrenic Nerve Burst Amplitude and Transiently Depresses Phrenic Nerve Burst Frequency

(A) Breeding scheme for ChR2$^+$ mice. Schematic for optogenetic stimulation of LepRb NTS neurons.

(B) EYFP$^+$ LepRb NTS neurons in the coronal plane (AP, area postrema; CC, central canal; 12N, 12th hypoglossal nuclei). Left panel scale bar, 100 μm; right panel scale bar, 20 μm.

(C) LepRb NTS neurons co-expressing EYFP (dark-blue immunostaining) and LepRb mRNA (dark-brown puncta). Scale bar, 20 μm.

(D) Schematic for optogenetic stimulation of LepRb NTS neurons.

(E) Representative traces of phrenic burst rate, heart rate, and integrated phrenic amplitude in ChR2$^+$ mice. Scale bar, 5 min.

(F) Representative traces of phrenic burst rate, heart rate, and integrated phrenic amplitude in ChR2^{-} mice. Scale bar, 5 min.
(G) Effect of light stimulation on phrenic burst rate (*f*) in ChR2^{-} and ChR2^{+} mice (control: n = 6; experimental group: n = 9).
(H) Effect of light stimulation on peak integrated phrenic burst amplitude ($\int$Phr) in ChR2^{-} and ChR2^{+} mice ($F_{(12, 156)} = 4.87$, $p < 0.0001$; control: n = 6; experimental group: n = 9).
(I) Effect of light stimulation on phrenic burst rate during first light stimulation in ChR2^{-} and ChR2^{+} mice ($F_{(2, 46)} = 15.39$, $p < 0.0001$; control: n = 12; experimental group: n = 13).
(J) Effect of light stimulation on integrated phrenic burst amplitude during first light stimulation in ChR2^{-} and ChR2^{+} mice (control: n = 12; experimental group: n = 13).
(K) Comparison of integrated phrenic amplitude between baseline and 35 min after light stimulation in ChR2^{+} mice. ($p = 0.0039$; control: n = 12; experimental group: n = 13).
(L) Comparison of phrenic burst rate between baseline and 35 min after light stimulation in ChR2^{-} mice ($p = 0.8438$; control: n = 12; experimental group: n = 13). Error bars represent ±SEM; n = number of mice in behavioral studies; p values reported from two-way repeated-measures (RM) ANOVA and Bonferroni post tests in (G). *$p < 0.05$, **$p < 0.01$, #$p < 0.001$ or Wilcoxon matched pairs signed-rank test in (J) and (K). **$p < 0.01$.

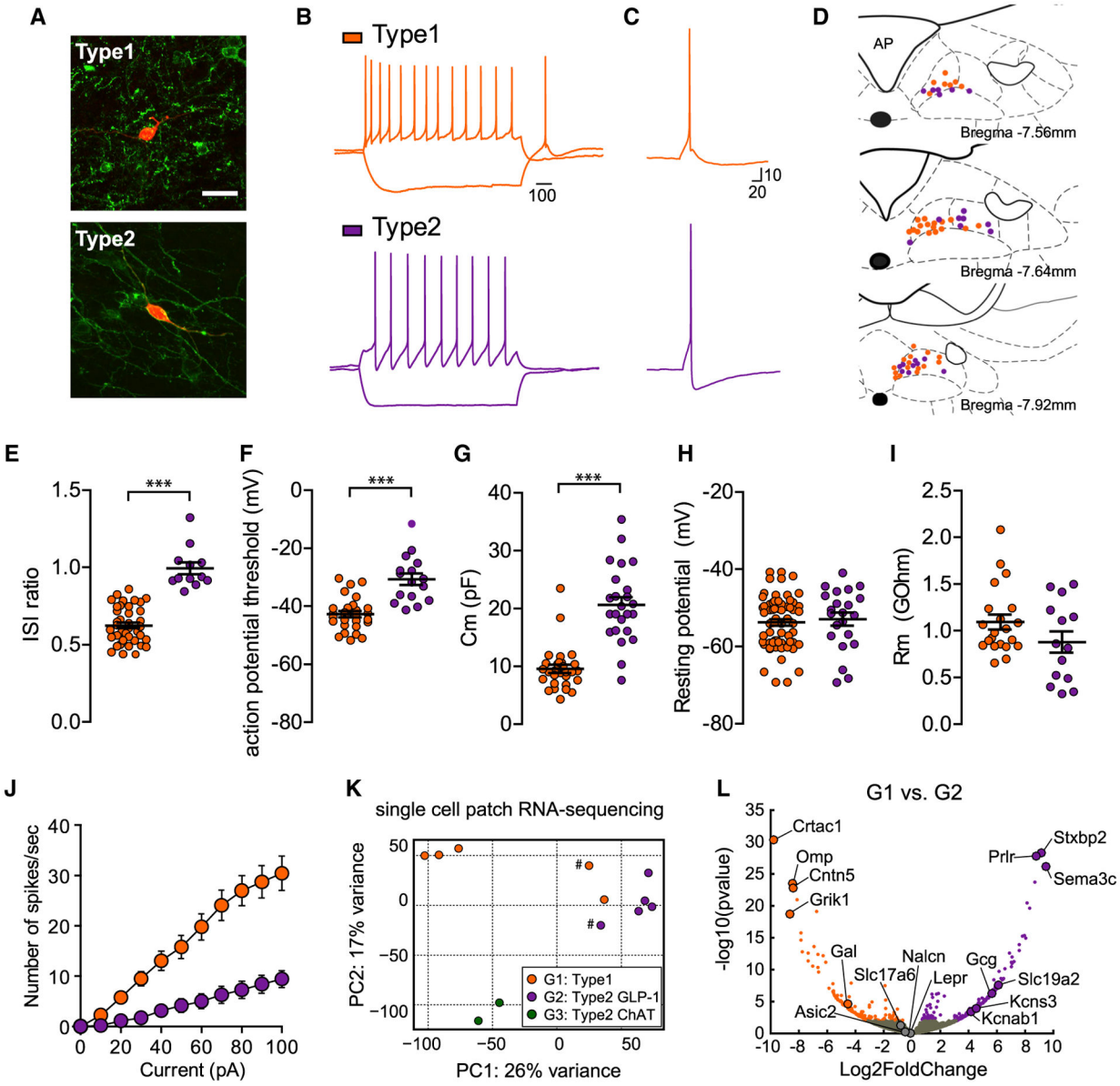

Figure 2. Intrinsic Electrophysiological Properties Identify Two Types of LepRb NTS Neurons

(A) Images of type-1 and type-2 LepRb NTS neurons (green) recorded and filled with biocytin (red). Scale bars, 30 μm.

(B) Current clamp recordings of the responses to a 50 pA of depolarizing current from a resting potential at −65 mV. Scale bar, 100 ms.

(C) Action potentials in response to a 5 ms (for type 1) or 7 ms (for type 2), 100 pA of depolarizing current. Horizontal scale bar, 20 ms; vertical scale bar, 10 mV.

(D) Map of the recorded type-1 (orange) and type-2 (purple) cells in the NTS shows no spatial segregation (AP, area postrema).

(E) Inter-spike interval (ISI) ratio in type-1 and type-2 cells. $p < 0.0001$. Type 1 n = 40 from 12 animals; type 2 n = 12 cells from seven animals.

(F) Action potential thresholds in type-1 and type-2 cells. $p < 0.0001$. Type 1 n = 28 cells from eight animals; type 2 n = 16 cells from six animals.
(G) Membrane capacitance (Cm) in type-1 and type-2 cells. $p < 0.0001$. Type 1 n = 29 cells from nine animals; type 2 n = 24 cells from eight animals.
(H) Resting membrane potential (RMP) in type-1 and type- 2 cells. $p = 0.4438$. Type 1 n = 67 cells from 19 animals; type 2 n = 22 cells from eight animals.
(I) Membrane resistance (Rm) of type-1 and type-2 cells. $p = 0.1623$. Type 1 n = 21 cells from six animals; type 2 n = 14 cells from five animals.
(J) Input-output curves of type-1 and type-2 cells. $p < 0.0001$, $F_{(1, 293)} = 36.368$. Type 1 n = 20 from five animals; type 2 n = 7 cells from five animals.
(K) Principal component analysis of single-cell RNA sequencing (RNA-seq) samples (n = 5 type-1 and n = 7 type-2 cells from seven animals). G1 represents type-1 cells, G2 represents type-2 cells, and G3 represents cholinergic cells. # indicates single-cell samples in which a low level of glia-specific genes were detected, possibly indicating contamination.
(L) A volcano plot of relative gene expression between type-1 and type-2 cells. Each point represents an individual gene. All genes differentially expressed in type-1 or type-2 cells with a false-discovery rate (FDR) of 0.05 are highlighted in either orange or purple. Type 1 n = 5; type 2 n = 5 cells, excluding cholinergic group-3 cells.
All error bars represent ±SEM; n is the number of cells; p values reported from Mann-Whitney U test in (E)-(I); ***$p < 0.001$ and linear regression in (J).

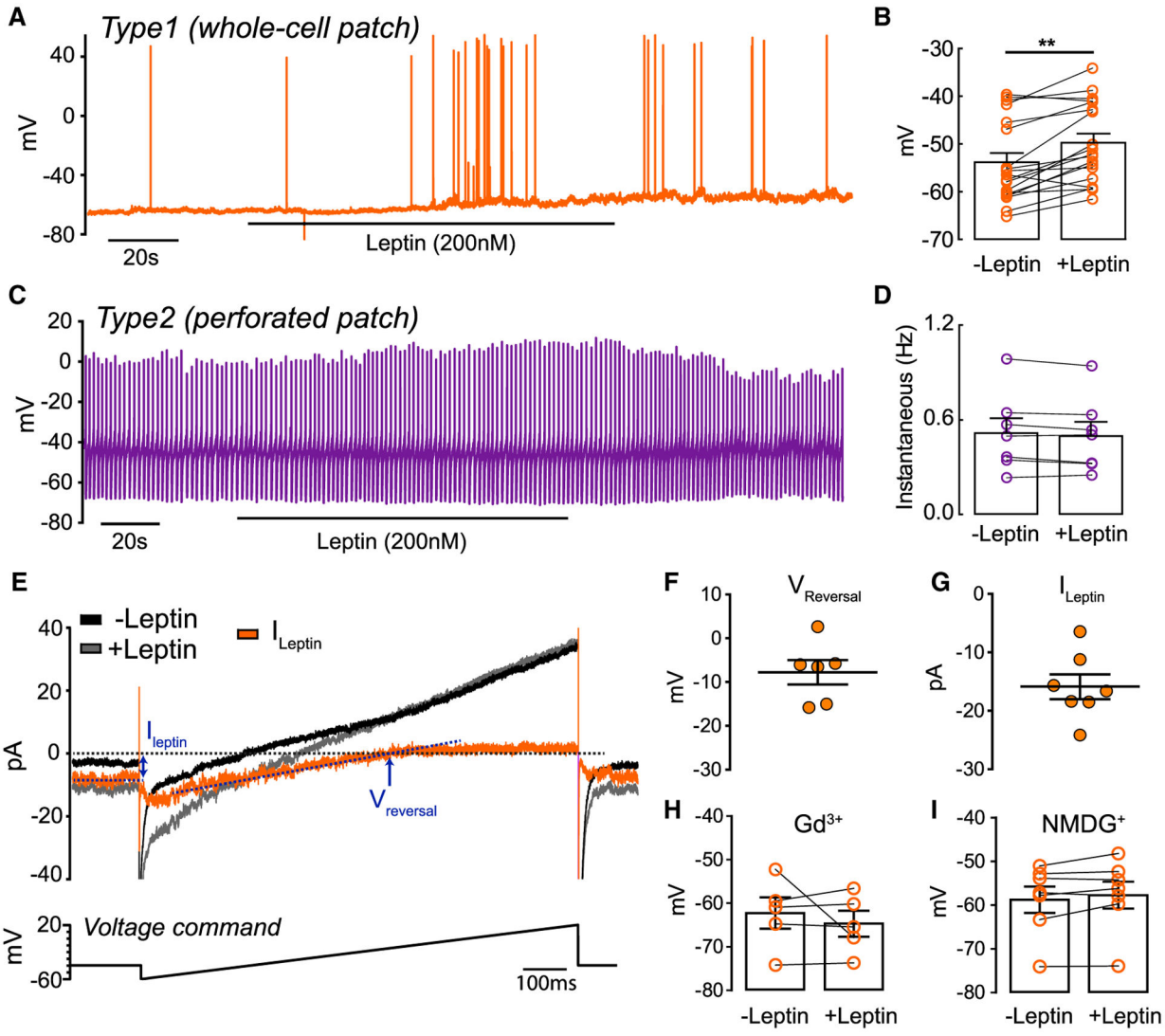

Figure 3. Leptin Selectively Depolarizes Type-1 Cells by Activating a Cationic Current

(A) Whole-cell slice recording showing the voltage response of a type-1 cell to focal leptin application.

(B) Summary of the leptin effect on membrane potential in type-1 LepRb NTS neurons. **p = 0.001, n = 19 cells from nine animals.

(C) Perforated-patch recording shows the lack of response from type-2 cells to focal leptin application.

(D) Summary of the effect of leptin on instantaneous firing rate in type-2 cells. p = 0.1094, n = 7 cells from five animals.

(E) Voltage-clamp recording of a type-1 cell before (black) and after (gray) leptin application. The leptin-evoked current (orange) was obtained by an offline digital subtraction of the control trace from the trace obtained in the presence of leptin.

(F) Mean reversal potential of the leptin-evoked current in type-1 cells (n = 5 cells from three animals).

(G) Mean amplitude of the leptin-evoked current in type-1 cells (n = 5 cells from three animals).
(H) Leptin-evoked depolarization of type-1 cells was abolished when Gd^{3+} (10 μM) was added to the extracellular solution. p = 0.5076, n = 5 cells from three animals.
(I) Leptin-evoked depolarization of type-1 cells was abolished when extracellular Na^{+} was substituted by NMDG. p = 0.2188, n = 7 cells from four animals. Error bars represent ±SEM; n represents number of cells; p values reported from Wilcoxon matched-pairs signed-rank test in (B), (D), (H), and (I). **p < 0.01.

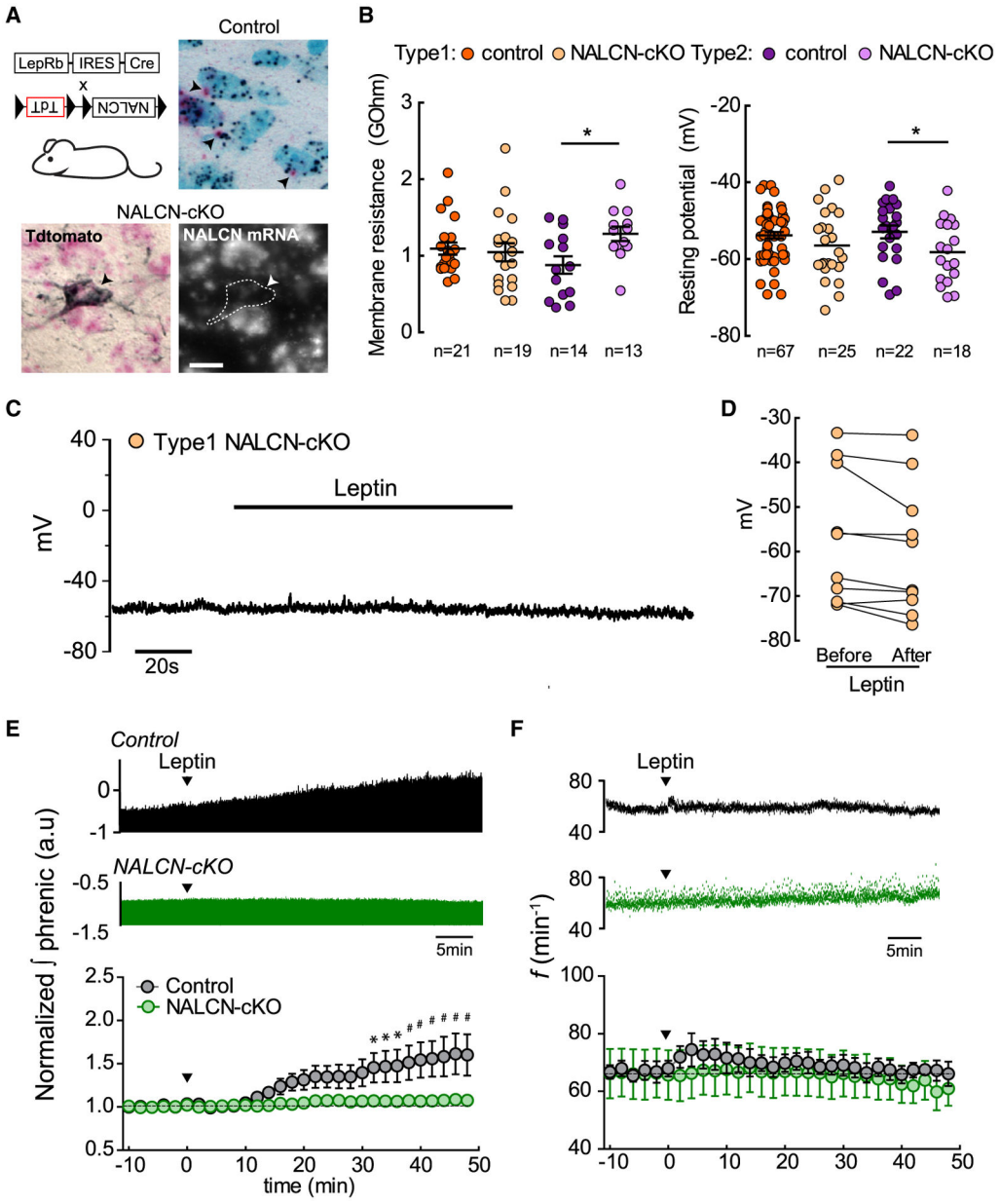

Figure 4. Leptin Activates NALCN to Stimulate Respiratory Motor Output

(A) Top left: breeding schemes for NALCN-cKO mice. Top right: LepRb mRNA (magenta puncta) and NALCN mRNA (blue puncta) in the NTS of control littermates. Bottom left: NALCN mRNA (magenta) and Tdtomato (blue, immunostaining) in the NTS of NALCN-cKO mice. Bottom right: NALCN mRNA (white) is not expressed in a Tdtomato^{+} LepRb neuron. Scale bars, 10 μm.

(B) Effect of NALCN deletion on the membrane resistance (type 2, *p = 0.0273) and resting potential (type 2, *p = 0.0457) of both cell types.

(C) Current clamp recording showing no effect of leptin (200 nM) application in a type-1 LepRb NTS neuron in a slice from a NALCN-cKO mouse.

(D) Summary of the leptin effect on the membrane potential in type-1 LepRb NTS neurons from NALCN-cKO mice. n = 10 cells from five mice.

(E) Top: representative trace of integrated phrenic nerve amplitude in control (black) and NALCN KO (green) mice. Bottom: effect of leptin injected into the NTS on integrated phrenic amplitude in control and NALCN KO groups. $F_{(27, 189)} = 5.75$, $p < 0.0001$; control, n = 4; NALCN-cKO, n = 5.

(F) Top: representative trace of phrenic burst frequency in control and NALCN-cKO mice. Bottom: effect of leptin injected into the NTS on phrenic burst rate. Control, n = 4; NALCN-cKO, n = 5.

Error bars represent ±SEM; n represents number of cells in (B) and (D) or number of animals in (E) and (F). p values reported from Mann and Whitney U test in (B) or two-way RM ANOVA and Bonferroni post tests in (E). $^{*}p < 0.05$ and $^{\#}p < 0.01$.

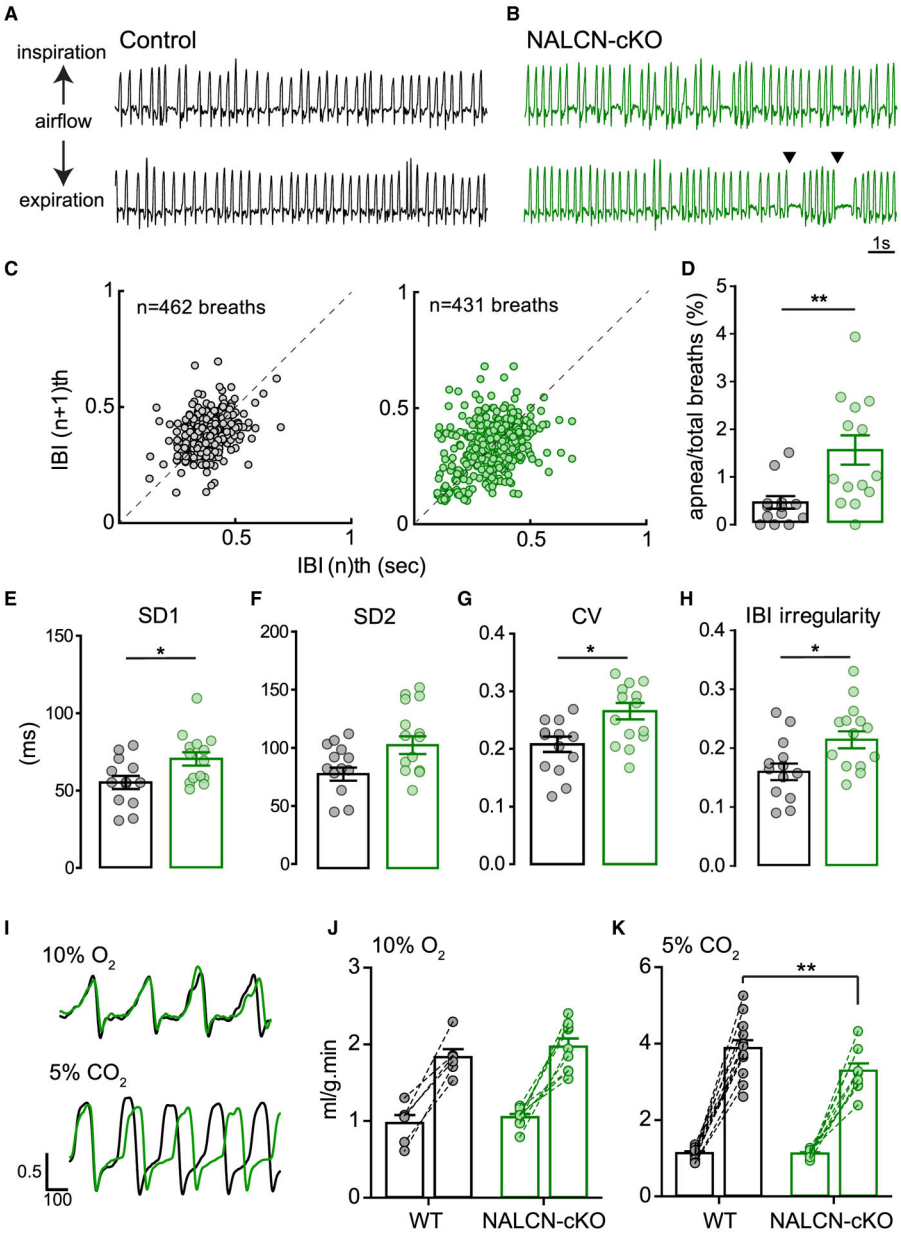

Figure 5. NALCN-cKO Mice Have Increased Breath-to-Breath Variability and Blunted Hypercapnic Ventilatory Response

(A) Whole-body flow-plethysmograph traces of control mice in quiet-awake state. Scale bar, 1 s.

(B) Whole-body flow-plethysmograph traces of NALCN-cKO mice in quiet-awake state (arrows indicate spontaneous apnea).

(C) Poincaré plots of inter-breath intervals (IBIs) in control and NALCN-cKO mice.

(D) Effect of NALCN deletion on spontaneous apnea occurrence. **p = 0.0022; control, n = 13; NALCN-cKO, n = 15.

(E) Effect of NALCN deletion on short-term variability (SD1) in IBIs. *p = 0.0341; control, n = 13; NALCN-cKO, n = 15.

(F) Effect of NALCN deletion on long-term variability (SD2) in IBIs. p = 0.053; control, n = 13; NALCN-cKO, n = 15.
(G) Effect of NALCN deletion on the coefficient of variation (CV) of IBIs. *p = 0.0213; control, n = 13; NALCN-cKO, n = 15.
(H) Effect of NALCN deletion on IBI irregularity. *p = 0.0146; control, n = 13; NALCN-cKO, n = 15.
(I) Representative whole-body plethysmograph airflow traces of control and NALCN-cKO in response to hypoxic (10% O_2) or hypercapnic (5% CO_2) gas challenges.
(J) Minute ventilation in response to hypoxia in control and NALCN-cKO mice. $F_{(1, 14)}$ = 0.08; control, n = 7; NALCN-cKO, n = 9.
(K) Minute ventilation in response to hypercapnia in control and NALCN-cKO mice. $F_{(1,20)}$ = 6.79; interaction p = 0.0169; control, n = 10; NALCN-cKO, n = 12. Error bars represent ±SEM; n represents number of animals; p values reported from Mann and Whitney U test in (D)-(H). *p < 0.05 or two-way ANOVA RM in (J) and (K) and Bonferroni post tests in (K). **p < 0.01.

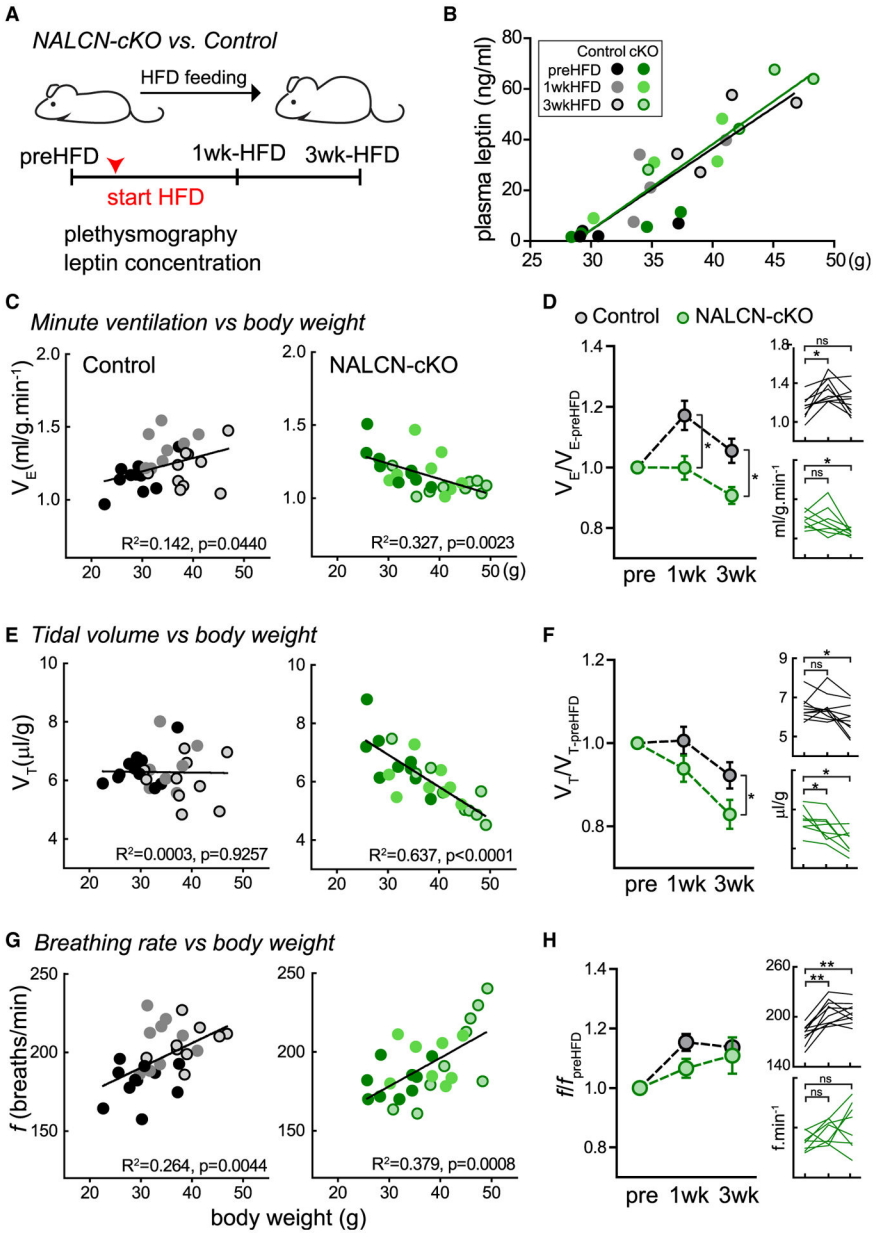

Figure 6. NALCN-cKO Mice Do Not Match Ventilation to HFD-Induced Changes in Body Weight

(A) Schematic and timeline for HFD feeding and measures of breathing.

(B) Plasma leptin concentration versus body weight (see also Figure S6). Control group, n = 4; NALCN-cKO group, n = 4.

(C) Correlation between minute ventilation and body weight in control (left panel, p = 0.044, n = 10) and NALCN-cKO mice (right panel, p = 0.0023, n = 8). Lines represent best fit of linear regression. Control group, $F_{(1, 27)} = 4.47$; NALCN-cKO group, $F_{(1, 24)} = 11.68$.

(D) Effect of HFD on minute ventilation in control and NALCN-cKO mice. $F_{(2, 47)} = 3.79$; p = 0.0298. Insets show minute ventilation of individual animals in control (1-wk p = 0.0015; n = 10) and NALCN-cKO (3-wk p = 0.0391; n = 8) groups.

(E) Correlation between tidal volume and body weight in control ($p = 0.9257$) and NALCN-cKO ($p < 0.0001$) mice. Lines represent best fit of linear regression. NALCN-cKO group, $F_{(1, 24)} = 42.15$.
(F) Effect of HFD on tidal volume in control and NALCN-cKO mice. $F_{(2.47)} = 7.38$; $p = 0.0016$. Insets show tidal volume of individual animals in control (3-wk $p = 0.0488$) and NALCN-cKO (1-wk $p = 0.0391$; 3-wk $p = 0.0156$) groups.
(G) Correlation between breathing frequency and body weight in control mice ($p = 0.0044$) and NALCN-cKO mice ($p = 0.0008$). Lines represent best fit of linear regression. Control group, $F_{(1, 27)} = 9.68$; NALCN-cKO group, $F_{(1, 24)} = 14.66$.
(H) Effect of HFD on breathing frequency in control and NALCN-cKO mice. Insets show breathing frequency of individual animals in control (1-wk $p = 0.0039$, 3-wk $p = 0.0039$) and NALCN-cKO groups.
Error bars represent ±SEM; n is number of animals; p values reported from two-way ANOVA test in (D) and (F) and Wilcoxon signed-rank tests in insets of (D), (F), and (H). *$p < 0.05$, **$p < 0.01$.

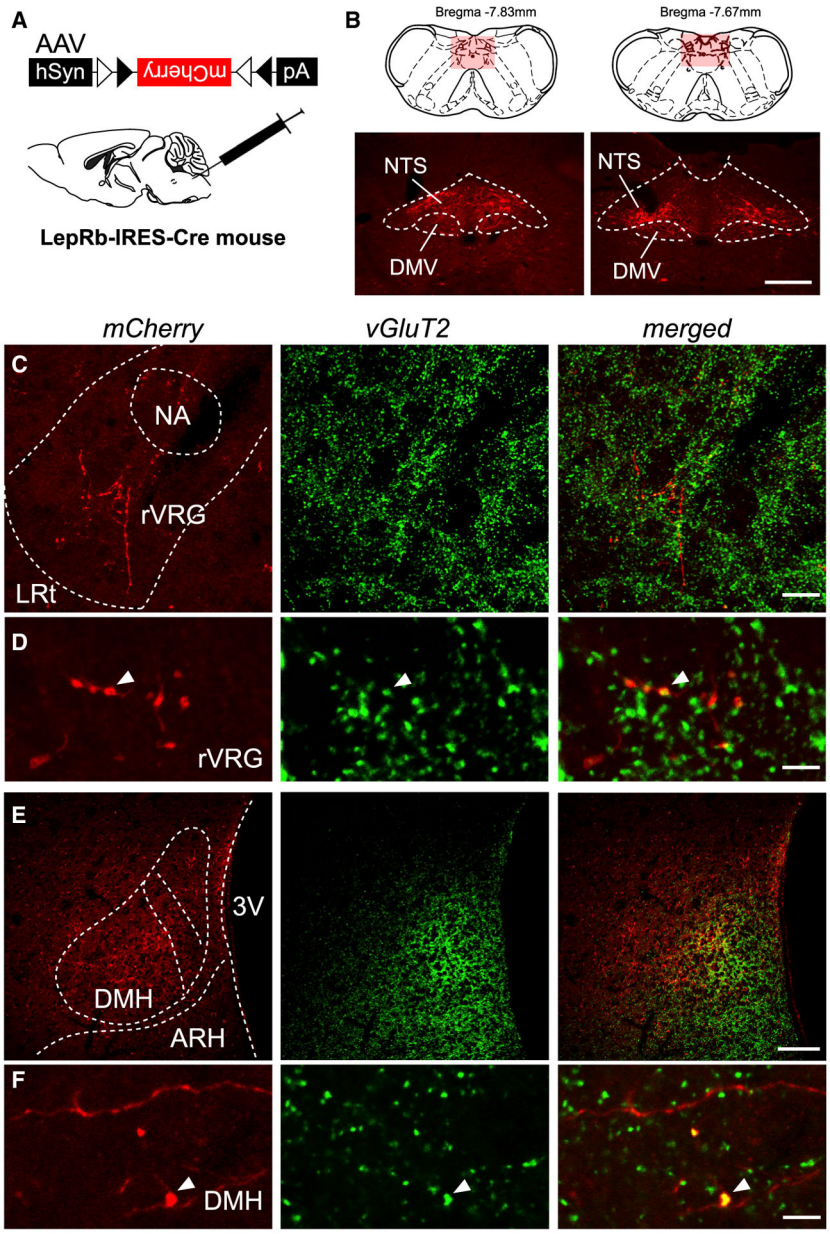

Figure 7. VGluT2-Expressing LepRb NTS Neurons Project to the rVRG and the DMH

(A) Schematic of viral injection into NTS for anterograde tracing of LepRb NTS neurons (n = 3 mice).

(B) Bilateral mCherry expression in LepRb NTS neurons. (DMV, dorsal motor nucleus of the vagus). Scale bar, 200 μm.

(C) mCherry-expressing axon terminals (red, left panel) and VGluT2 expression (green, middle panel) in the rVRG (merged, right panel). Scale bar, 20 μm.

(D) Higher magnification showing colocalization of mCherry-expressing axon terminals (red, left panel) and VGluT2 (green, middle panel) in the rVRG (merged, right panel). Scale bar, 5 μm.

(E) mCherry-expressing axon terminals (red, left panel) and VGluT2 expression (green, middle panel) in the DMH (merged, right panel). Scale bar, 100 μm.
(F) Higher magnification showing colocalization of mCherry-expressing axon terminals (red, left panel) and VGluT2 (green, middle panel) in the DMH (merged, right panel). Scale bar, 5 μm.

KEY RESOURCES TABLE

REAGENT or RESOURCE	SOURCE	IDENTIFIER
Antibodies		
Chicken polyclonal GFP antibody (1:2000)	Abcam	Cat.# ab13970; RRID:AB_300798
Chicken polyclonal mCherry antibody (1:2000)	Abcam	Cat.# ab205402; RRID:AB_2722769
Rabbit GFP antibody (1:5000)	Millipore	Cat.# AB3080; RRID:AB_91337
Rabbit polyclonal pSTAT3 antibody (1:500)	Cell Signaling Technology	Cat.# 9131; RRID:AB_331586
Rabbit c-Fos antibody (1:1000)	Millipore	Cat.# ABE457; RRID:AB_2631318
Guinea pig polyclonal VGluT2 antibody (1:5000)	Millipore	Cat.# AB2251-I; RRID:AB_2665454
Guinea pig polyclonal VGluT2 antibody (1:500)	Synaptic Systems	Cat.# 135404; RRID:AB_887884
Goat anti-rabbit Alexa 488 (1:600)	Invitrogen	Cat.# A-11034; RRID:AB_2576217
Goat anti-chicken Alex 488 (1:600)	Invitrogen	Cat.# A-11039; RRID:AB_2534096
Goat anti-rabbit Alexa 594 (1:600)	Invitrogen	Cat.# A-11012; RRID:AB_2534079
Goat anti-chicken Alexa 594 (1:600)	Invitrogen	Cat.# A-11042; RRID:AB_2534099
Goat anti-guinea pig Alexa 647 (1:600)	Invitrogen	Cat.# A-21450; RRID:AB_2735091
Bacterial and Virus Strains		
pAAV-hSyn-DIO-hM4D(Gi)-mCherry	Krashes et al., 2011	RRID:Addgene_44362
Chemicals, Peptides, and Recombinant Proteins		
Proteinase K	Sigma-Aldrich	Ref. 0311588701
Mouse Leptin	National Hormone and Peptide Program	Dr. A.F. Parlow
SG substrate kit peroxidase	Vector laboratories	Cat.# SK-4700; RRID:AB_2314425
Vectamount	Vector laboratories	Cat.# H-5000; RRID:AB_2336786
Critical Commercial Assays		
Mouse Leptin ELISA kit	Crystal Chem, USA	Cat.# 90030
SMART-Seq v4 Ultra Low Input RNA Kit for Sequencing	Takara Bio, USA	Cat.# 634894
Nextera XT DNA Library Preparation Kit	Illumina, USA	FC-131–1024
RNAscope 2.5 High Definition BROWN Assay kit	Advanced Cell Diagnostics, USA	Cat.# 322371
RNAscope 2.5 Duplex Assay kit	Advanced Cell Diagnostics, USA	Cat.# 322436
Deposited Data		
LepRb NTS type1 and type2 single-cell RNA- sequencing data	Gene Expression Omnibus	GSE158582
Experimental Models: Organisms/Strains		
B6.129(Cg)-Lepr$^{tm2(cre)Rck}$/J	Jackson Laboratories, USA	RRID:IMSR_JAX:008320
B6;129S-Gt(ROSA)26Sor$^{tm32(CAG-COP4*H134R/EYFP)Hze}$/ J (Ai32)	Jackson Laboratories, USA	RRID:IMSR_JAX:024109
B6;129S-Gt(ROSA)26Sor$^{tm39(CAG-hop/EYFP)Hze}$/J (Ai39)	Jackson Laboratories, USA	RRID:IMSR_JAX:014539
C57;B6 loxP-Tdt::loxP-NALCN	Deijen Ren, UPenn	Lu et al., 2007
Oligonucleotides		
Mm-Gcg-O1	Advanced Cell Diagnostics, USA	Ref. 482311
Mm-CCK	Advanced Cell Diagnostics, USA	Ref. 402271
Mm-POMC	Advanced Cell Diagnostics, USA	Ref. 314081
Mm-Gal	Advanced Cell Diagnostics, USA	Ref. 400961

REAGENT or RESOURCE	SOURCE	IDENTIFIER
Mm-Gal-C2	Advanced Cell Diagnostics, USA	Ref. 400961-C2
Mm-NALCN	Advanced Cell Diagnostics, USA	Ref. 415161
Mm-Lepr	Advanced Cell Diagnostics, USA	Ref. 402731
Mm-Lepr-tv1-C2	Advanced Cell Diagnostics, USA	Ref. 471171-C2
Software and Algorithms		
Clampfit10.2	Axon Instruments	https://www.moleculardevices.com
MATLAB	MathWorks	https://www.mathworks.com
Prism5	GraphPad	https://www.graphpad.com
Other		
Temperature transponder	BMDS, USA	IPTT-300